A&A 489, 849–883 (2008)
DOI: 10.1051/0004-6361:200809685

Astronomy & Astrophysics

A revised catalogue of EGRET γ-ray sources

J.-M. Casandjian and I. A. Grenier

Laboratoire AIM, CEA/DSM, CNRS, Université Paris Diderot, Service d'Astrophysique, CEA Saclay, 91191 Gif-sur-Yvette, France
e-mail: [casandjian@cea.fr;isabelle.grenier]@cea.fr

Received 29 February 2008 / Accepted 23 May 2008

ABSTRACT

Aims. We present a catalog of point γ-ray sources detected by the EGRET detector on the Compton Gamma Ray Observatory. We used the entire γ-ray dataset of reprocessed photons at energies above 100 MeV and new Galactic interstellar emission models based on CO, HI, dark gas, and interstellar radiation field data. Two different assumptions are used to describe the cosmic-ray distribution in the Galaxy to analyse the systematic uncertainties in source detection and characterization.
Methods. We applied a 2-dimensional maximum-likelihood detection method similar to that used to analyze the 3rd EGRET catalogue.
Results. The revised catalogue lists 188 sources, 14 of which are marked as confused, in contrast to the 271 entries of the 3rd EGRET (3EG) catalogue. We do not detect 107 sources discovered previously because additional structure is present in the interstellar background. The vast majority of them were unidentified and marked as possibly extended or confused in the 3EG catalogue. In particular, we do not confirm most of the 3EG sources associated with the local clouds of the Gould Belt. Alternatively, we found 30 new sources that have no 3EG counterpart. The new error circles for the confirmed 3EG sources largely overlap the previous ones, but several counterparts of particular interest discussed before, such as Sgr A*, radiogalaxies, and several microquasars are now found outside the error circles. We cross-correlated the source positions with a large number of radio pulsars, pulsar wind nebulae, supernova remnants, OB associations, blazars and flat radiosources and we found a surprising large number of sources (87) at all latitudes that have no counterpart among the potential γ-ray emitters.

Key words. catalogs – gamma rays: observations – ISM: structure

1. Introduction

The Energetic Gamma-Ray Experiment Telescope (EGRET), which operated onboard the Compton-Gamma Ray Observatory from April 1991 to May 2000, detected photons in the 20 MeV to 30 GeV range. The observation program made use of the large instrumental field of view (25° in radius) to cover the entire sky and complete in-depth studies of specific regions. The corresponding exposure and flux sensitivity to point sources are therefore not uniform across the sky. The sensitivity threshold also varies because of the intense background emission that arises from cosmic-ray interactions with the interstellar gas and photon fields in the Milky Way. The minimum flux detectable by EGRET rises steeply with decreasing Galactic latitude. To be able to detect point sources and assess their significance in these varying conditions, a 2-dimensional maximum-likelihood method using binned maps was developed for analyzing the COS-B data (Pollock et al. 1981) and implemented in the study of EGRET data set (Mattox et al. 1996). A first catalog generated with this method was published for the first 1.5 years of data (Fichtel et al. 1994), followed by the second one (Thompson et al. 1995), and its supplement (Thompson et al. 1996) after 3 years of data. Lamb & Macomb (1997) presented a catalog of sources detected above 1 GeV. The last EGRET catalog (hereafter 3EG, Hartman et al. 1999) comprised reprocessed data from April 1991 to October 1995 and the interstellar emission model from Hunter et al. (1997) and extragalactic background from Sreekumar et al. (1998). This version contained 271 point sources including a solar flare, the Large Magellanic Cloud, five pulsars, one radiogalaxy detection (Cen A), 66 high-confidence identifications of blazars (BL Lac objects and flat-spectrum radio quasars), and 27 lower-confidence blazar identifications. Because of the wide tails of the instrument point-spread function, seven potential artifacts were noted around the brightest sources and many sources were marked as confused or possibly extended.

The 3EG catalogue also contained 170 sources with no attractive counterpart at lower energy. About 130 of them remain unidentified (see Grenier (2004) and references therein). Candidate counterparts included pulsars and their wind nebulae, supernova remnants, massive stars, X-ray binaries and microquasars, blazars and nearby radiogalaxies, luminous infrared and starburst galaxies, and galaxy clusters. It was also noticed (Grenier 1995; Grenier 2000; Gehrels et al. 2000) that the most stable unidentified sources were correlated significantly with the nearby Gould Belt, a system of massive stars and interstellar clouds that surrounds the Sun at a distance of hundreds of parsecs. The offset position of the Sun with respect to the Belt centre and the Belt inclination of 17° with respect to the Galactic plane provides a useful spatial signature across the sky (Perrot & Grenier 2003).

EGRET continued to observe for an additional 4.5 years following the 4 cycles used in the 3EG analysis. Its sensitivity was reduced because of the ageing gas in the spark chamber, but it gathered almost an additional ten percent of photons and detected several new variable sources. Several authors (Nolan et al. 2003; Sowards-Emmerd et al. 2005), however, noticed discrepancies between their studies and at least five 3EG

sources. They failed to confirm some and found additional. The entire γ-ray dataset and final instrument response functions were also reprocessed significantly by the EGRET team in 2001. Furthermore, the spatial coverage of CO surveys has reached higher latitudes since 1999, finding new small CO clouds (Dame et al. 2001). In parallel, new HI surveys (Kalberla et al. 2005) have been completed to correct for the significant contamination of stray radiation present in the older surveys. Finally, an additional 'dark' gas component was discovered in the Gould Belt clouds that increased their estimated mass and spatial extent significantly (Grenier et al. 2005). The additional mass is structured into large envelopes around the dense CO cores, and does not follow the HI and CO maps commonly used to trace atomic and molecular column-densities. The dark gas therefore provides both γ-ray intensity and structure that were not accounted for in the 3EG background model.

For all of these reasons and in preparation for the new GLAST mission, the interstellar background model had to be revised and the EGRET detection method was applied to the full nine years of data to build a revised catalogue of sources above 100 MeV. To study the systematic uncertainties in source locations and fluxes due to our limited knowledge of the intense interstellar background, we applied our analysis to two different background models, exploiting the same new interstellar data, but using independent approaches to constrain the cosmic-ray gradient across the Galaxy.

2. The Galactic interstellar emission models

The high-energy Galactic emission is produced by the interaction of energetic cosmic-ray electrons and protons with interstellar nucleons and photons. The decay of neutral pions produced in hadron collisions accounts for most of the emission above 300 MeV. Inverse Compton (IC) scattering of the interstellar radiation field by electrons and their bremsstrahlung emission in the interstellar gas are the other main contributors to the Galactic emission. The observed intensity therefore scales with the integral along the line-of-sight of the product of the cosmic-ray density and the gas or soft-photon density.

The diffuse model used to produce the 3EG catalogue (Hunter et al. 1997) was based on a 3D-distribution of matter, cosmic-ray, and soft-photon densities in the Galaxy, where the cosmic-ray density was assumed to be coupled to the gas density over a given length scale. This length scale and the CO-to-$H2$ conversion factor (X ratio) were adjusted to the data. The 3D gas map was obtained from the HI and CO line surveys and from kinematical distances derived for circular rotation. Distance ambiguities in the inner Galaxy were solved by dividing the gas into the far and near sides according to its expected scale height. Gas with velocities in excess of the tangent values was attributed to the tangent point; the gas emission within 10° of both the Galactic centre and anticentre was interpolated from the regions just outside these boundaries and normalized to match the total emission observed along the line-of-sight. The resulting map is, however, still strongly biased to our side of the Galaxy, particularly for the atomic gas. This bias is reflected in the cosmic-ray density via the coupling length.

For the present analyses, we assumed an axisymmetric Galaxy for the cosmic-ray density and we used gas column-density distributions in Galactocentric rings that are less affected by biases caused by the strategy adopted to measure the cloud distance in the inner Galaxy. The radial velocity information in the HI and CO line surveys together with the rotation curve of Clemens (1985) and the solar motion parameters ($v = 220$ km s^{-1} at $R = 8.5$ kpc), were used to partition the gas into 6 rings bounded by 3.5, 7.5, 9.5, 11.5, and 13.5 kpc in Galactocentric distance (Digel et al., in preparation). Gas within 10° of the Galactic centre and anticentre was interpolated as before. The all-sky Leiden-Argentina-Bonn (LAB) composite survey (Kalberla et al. 2005) was used for the HI data. Column densities, N(HI), were derived by assuming a constant spin temperature of 125 K. The velocity-integrated CO brightness temperature, W(CO), was taken from the Center for Astrophysics compilation of observations at $|b| \leq 32°$ (Dame et al. 2001). The regions outside the survey boundaries should be free of bright CO emission.

We used two different approaches to account for the cosmic-ray density gradient. One is based on the Galprop model for cosmic-ray propagation developed by Strong et al. (2007, 2004a, 2004b), using run number 49-6002029RB to derive the γ-ray maps from pion decay, I_{π^0}, bremstrahlung radiation, $I_{\rm brem}$, and inverse Compton radiation, $I_{\rm IC}$. This version includes secondary electrons and positrons, an optimized cosmic-ray spectrum to reproduce the GeV excess in the EGRET data, a cosmic-ray source distribution matching the radial profile of pulsars and supernova remnants, a radial gradient in the X factor, and the new HI and CO gas rings.

The second model, hereafter referred to as the Ring model, is based on the simpler, but realistic hypothesis that, if energetic cosmic rays penetrate uniformly all gas phases, the γ-ray intensity in each direction can be modelled by a linear combination of gas column-densities in the different rings, plus the IC intensity map (as predicted by Galprop), and an isotropic intensity ($I_{\rm iso}$) that accounts for local IC emission and extragalactic emission. This assumption was used to derive gas emissivities in several rings from the COS-B and EGRET data (Strong et al. 1988; Strong & Mattox 1996). We repeated these analyzes to derive gas emissivities for the new HI and CO rings using 9 years of EGRET data in three energy bands (>100 MeV, 0.3–1 GeV, >1 GeV). Both the Ring and Galprop models used the revised distribution of the interstellar radiation field (Porter & et al. 2005; Moskalenko et al. 2006) to calculate the IC intensity map. The Galprop IC map is common to both diffuse models.

As indicated in the introduction, we also included in the local ring the large column-densities of "dark" gas associated with cold and anomalous dust at the transition between the atomic and molecular phases (Grenier et al. 2005). This transitional phase is not traced in the radio. After removing from total dust column-density maps the part that correlates linearly with N(HI) and W(CO), large envelopes of excess dust remain surrounding nearby CO. The fact that the excess dust correlates spatially with significant diffuse gamma radiation indicates that cosmic rays pervade gas not accounted for in HI or CO. As inferred from the excess dust and correlated γ-ray data, the gas-to-dust ratio in this phase is normal. This phase appears to form an extended layer at the transition between the dense CO cores and the densest parts of the outer HI envelope of a cloud complex. It is observed most clearly in total dust maps such as the reddening $E(B-V)$ map (Schlegel et al. 1998), or low-frequency thermal emission at 93 GHz for WMAP (Finkbeiner et al. 1999), or anomalous emission close to 20 GHz (Lagache 2003). We constructed a "dark" gas column-density template, $NH_{\rm dark}$, by removing from the $E(B-V)$ map the part that was correlated linearly with N(HI) and W(CO). This template was converted into gas column-densities by fitting the all-sky γ-ray maps with this template as well as N(HI) and W(CO) rings, IC and isotropic components. Because of its column-densities, clumpiness, and large spread across the sky (see Fig. 4 in Grenier et al. 2005), the

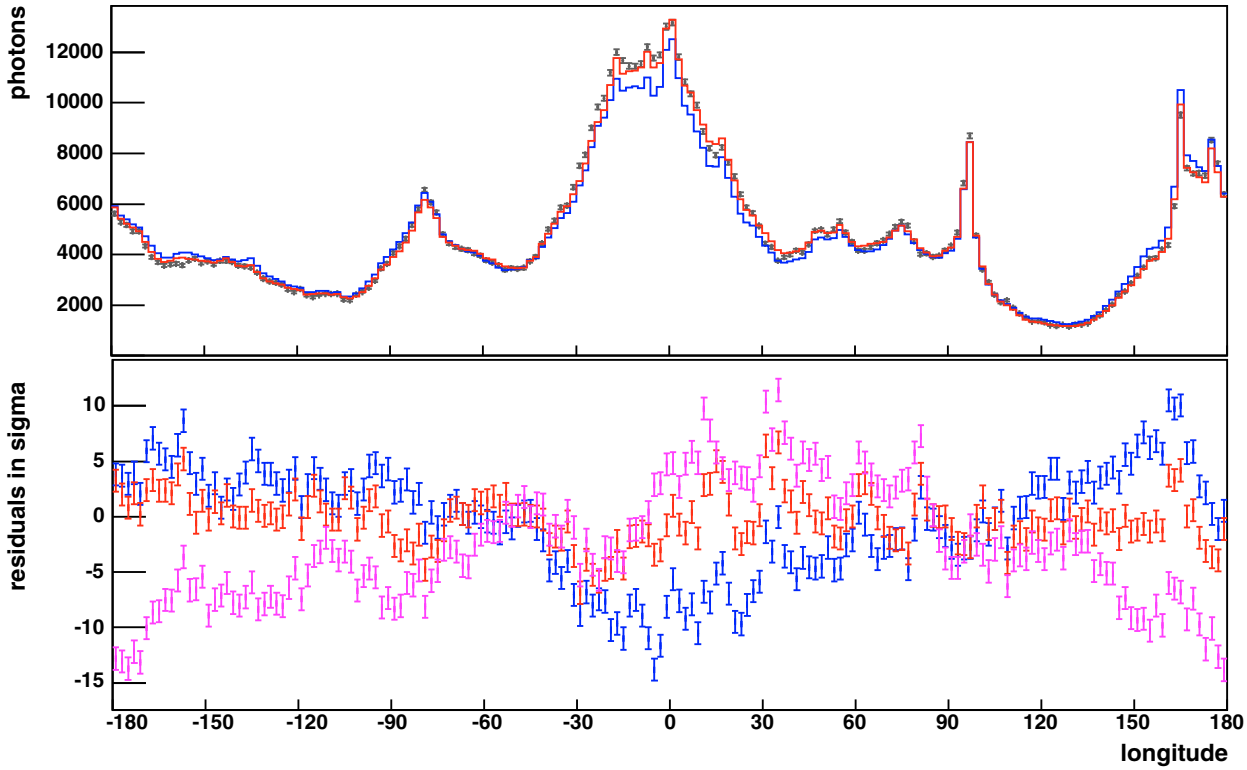

Fig. 1. *The top figure* is the longitude profile of all photon counts observed by EGRET above 100 MeV at all latitudes (black error bars), compared with the diffuse counts predicted by the 3EG model (blue curve) and the Ring model (red curve). *The bottom figure* is the residual expressed in number of standard deviation, colors are the same as above, we added the Galprop residuals in purple. Counts from bright sources have been added to the diffuse component. For more visibility the plot are presented with a binning of 4°.

"dark" gas component may strongly affect source detectability. This template was also added to the Galprop 49-6002029RB background model.

To summarize, two diffuse backgrounds were constructed by fitting different components to the EGRET photon maps, in $0.5° \times 0.5°$ bins, in the three energy bands that we use for source detection (>100 MeV, 0.3–1 GeV, >1 GeV). With the Ring model, the predicted count rates are calculated as:

$$\begin{aligned} N_{\rm pred}(l,b) &= [\Sigma_{i=\rm rings} q_{{\rm HI},i} N_{\rm HI}(r_i,l,b) + \Sigma_{\rm rings} q_{{\rm CO},i} W_{\rm CO}(r_i,l,b) \\ &\quad + q_{\rm dark} NH_{\rm dark}(l,b) + q_{\rm IC} I_{\rm IC}(l,b) + I_{\rm iso}] \times \epsilon(l,b) \\ &\quad + \Sigma_{j=\rm sources} \epsilon(l_j,b_j)\, f_j\, PSF(l_j,b_j) \end{aligned}$$

and the Galprop model as:

$$\begin{aligned} N_{\rm pred}(l,b) &= [q_{\pi^0} I_{\pi^0}(l,b) + q_{\rm brem} I_{\rm brem}(l,b) + q_{\rm dark} NH_{\rm dark}(l,b) \\ &\quad + q_{\rm IC} I_{\rm IC}(l,b) + I_{\rm iso}] \times \epsilon(l,b) \\ &\quad + \Sigma_{j=\rm sources} \epsilon(l_j,b_j)\, f_j\, PSF(l_j,b_j). \end{aligned} \quad (1)$$

In both models, $\epsilon(l,b)$ and f_j represent the EGRET exposure map and source fluxes respectively. The product of the diffuse maps and the exposure were convolved with the EGRET PSF for an input $E^{-2.1}$ spectrum before adding the source maps. The EGRET count and exposure maps, the 3EG diffuse model, as well as the latest instrument response functions, were downloaded from the CGRO Science Support Center. They differ from those used for 3EG since they were reprocessed in 2001. The q parameters (gas emissivities or relative contributions of different radiation components) were fitted to the data by means of a maximum likelihood with Poisson statistics. To avoid biasing the interstellar parameters, the model included the brightest sources detected during a first source detection iteration with a significance $>5\sigma$, with fixed fluxes. Changing these fluxes within their statistical uncertainties do not significantly change the diffuse results.

The resulting emissivities corresponding to the local gas are fully consistant with Table 1 of Grenier et al. (2005). The emissivity gradient in the Galactic plane will be described in a separate paper. The quality of the fit can be seen in Fig. 1. The top figure displays the longitude profile of all the EGRET photon counts above 100 MeV. The error bars are only statistical. The plot compares the best fit that can be obtained using the former 3EG diffuse model with the longitude profile resulting from the present Ring model. The bottom plot shows the longitude profile of the residuals and the improvement of the ring model over the 3EG one. It also shows the residuals for the best fit Galprop model. All modelled profiles include the brightest sources. Systematic differences can be seen in various places where the 3EG model significantly over predicts and under predicts the data while the new models describe the data more accurately. Because of its larger flexibility (the gas emissivity gradient due to cosmic-ray variations is measured, not inferred from propagation properties or gas coupling), the Ring model was found to best fit the data. We note than even if the agreement is excellent, there still exists small deviations that can significantly impact source detection and characterization.

The residual count map obtained above 100 MeV with the Ring model is presented in Fig. 2. It displays the statistical difference $(N_{\rm obs} - N_{\rm pred})/\sqrt{N_{\rm pred}}$ between the observed counts and those predicted from the diffuse background and bright sources using Eq. (1). The model globally fits the data very well. The extended blue fan-like structures with negative residuals are correlated with the edge of several observing periods. They are probably caused by an incorrect estimate of the exposure at large

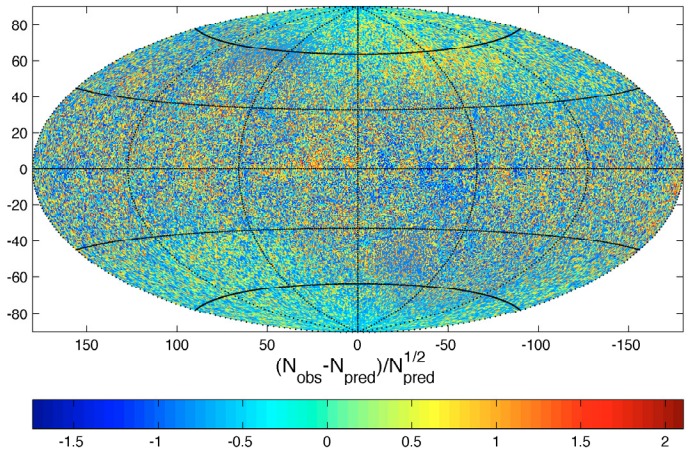

Fig. 2. Map in Galactic coordinates of the residuals (expressed in $\sigma = \sqrt{N_{\rm pred}}$ values) between the $E > 100$ MeV photon counts (in 0.5° bin) and the best-fit Ring model solution given by Eq. (1).

angles from the instrument axis. They are visible independently of the choice of diffuse model (Ring, Galprop, or 3EG). Their spatial extent is sufficiently large compared to the PSF size not to severely affect source detection, yet source fluxes in these directions are underestimated. Uncertain knowledge of the off-axis instrument exposure is also reflected in the small model deficit (orange edge) bordering the fan-like excesses. We checked for suspicious strings of faint sources that would correlate with these instrumental features.

The use of two different background models allowed us to study their impact on source detection and characterization. Given its higher likelihood value and locally flatter residuals, the Ring model was used to derive the default source flux and location. The values obtained with the Galprop background are used to illustrate the amplitude of the systematic uncertainty due to the background modelling. When searching for sources, we used the diffuse emission parameters calculated from this global fit. We adjusted the source flux and a free normalization of the total diffuse flux within 15° around each pixel, and a free isotropic flux. This procedure is the same as used for 3EG (Gmult and Gbias). These two parameters correct for small local mismatches between the diffuse model and the data. Gmult fluctuates around 1.

3. Source detection

As for deriving the 3EG catalogue, we used the LIKE code (Mattox 1996, version 5.61) to compute the 2-dimensional binned Poisson likelihood of detecting a source at a particular location on top of the diffuse background. LIKE calculates the Test Statistic (TS) value that compares the likelihood of detecting a PSF-like excess above the background to the null hypothesis – a random background fluctuation – for a given position. The likelihood (L_i) is calculated as the product, for all pixels within 15° of a specific position, of the Poisson probabilities of observing photons in a pixel where the number of counts is predicted by the model (background + source). The likelihood ratio test statistic is defined to be $TS = -2(LnL_0 - LnL_1)$, where the likelihood values L_1 and L_0 are optimized respectively with and without a source in the model. Asymptotically, the TS distribution follows a χ^2 one. The detection significance of a source at the given position is $\sqrt{TS}\sigma$ (Mattox 1996).

Sources were searched for in the summed maps corresponding to cycle 1, 2, 3, 4, 1 + 2, 3 + 4,1 + 2 + 3 + 4, 5 + 6, 7 + 8 + 9, 1 + 2 + 3 + 4 + 5 + 6 + 7 + 8 + 9. In addition, we analyzed the 46 individual periods listed in Table 1 for which flaring 3EG sources were detected. As for the summed maps, the individual period maps retained only photons with inclinations within 30° from the instrument axis, or 19° for cycle 6, 7, 8, and 9. Photons and exposure maps were binned to 0.5° × 0.5°.

To build the 3EG catalogue, sources were detected only in the integrated $E > 100$ MeV band. TS maps were then constructed in three energy bands (>100 MeV, 0.3–1 GeV, and >1 GeV) from the observation (single or summed) with highest TS and a source final position was obtained from the smallest error contours. Given the modern computer performance, we directly searched for sources independently in the three energy bands.

At 100 MeV, the EGRET PSF is wide and discrepancies exists between its real shape, as observed in bright sources, and its modelled one. In practice, differences may be caused because the source spectrum is more complex than the single power-law assumed to integrate the PSF. A choice of 300 MeV instead of 100 MeV for the lower analysis threshold might have provided a more effective compromise between count rates for detection and systematic uncertainties in the PSF. We, however, retained a lower limit of 100 MeV, as in 3EG, to account for soft sources and to allow comparison with the 3EG results. We assumed a spectral index of 2.0 for all sources, apart from 11 bright sources with a 3EG spectral index that differed significantly from 2.0, for which we integrated the PSF using their 3EG index.

Each of the 10 all-sky summed maps was divided, both in Galactic and equatorial coordinates, in 45 zones with a large overlap. The use of both coordinates systems is required since source images are deformed in rectangular projection at high latitude or declination. For each zone, each individual period, and each of the 3 energy bands (>100 MeV, 0.3–1 GeV, and >1 GeV), we calculated a TS map for excesses above the background. Sources were iteratively detected from high TS to low TS in successive TS maps. Between each steps, the detected sources were included in the background model until no excess with $\sqrt{TS} > 3$ remained in the final TS map. An example of the iteration around Geminga is given in Fig. 3. Peaks in the TS map were automatically detected with SExtractor (Bertin & Arnouts 1996) and converted into source positions by taking the TS-weighted centroid in the region enclosed by the 95% confidence contour around this position. Source positions were recalculated at each iteration to take into account the influence of the neighbouring sources. More than 1100 TS-maps were thus calculated at the CCIN2P3 Computing Center.

4. Catalogue construction

To account for real versus modelled PSF discrepancies in extremely bright sources, for instance to account for the splitting in two of the bright pulsar sources or for the artifacts in the Vela tails, we removed all source candidates within 3.5° of the intense sources (that exhibit more than 800 photons in a map). For less intense sources, we checked the probability of having a double versus single source with a specific likelihood calculation, using the likelihood ratio between the 2 cases to keep or reject the double source.

At the end of this stage, most sources have two possible positions per energy band and observation, one from the Galactic coordinate map and one from the equatorial one. We cross-compared the two and selected the position from the least

Table 1. List of individual or short periods used in the analysis in addition to the summed cycles.

Name	Sum of viewing periods	Name	Sum of viewing periods	Name	Sum of viewing periods
2+	0002+0003+0004+0005	2040		3315	
0020		virg2	2040+2050+2060	330+	3300+3320
0040		2110		335+	3350+3355
0050		2230		vrg3a	3040+3050+3060+3070+3080+3086
0200		2260		3355	
0210		227+	2270+2280	3360	
0220		229+	2290+2295	3385	
0230		2310		3390	
0250		3023		4040	
0260		314+	3140+3150	4100	
0290		3170		4130	
36+	0360+0365	319+	3190+3195	4180	
0420		3200		419+	4191+4195
0430		328+	3280+3310+3315+3330	4210	
0440		3290		4230	
				4235	

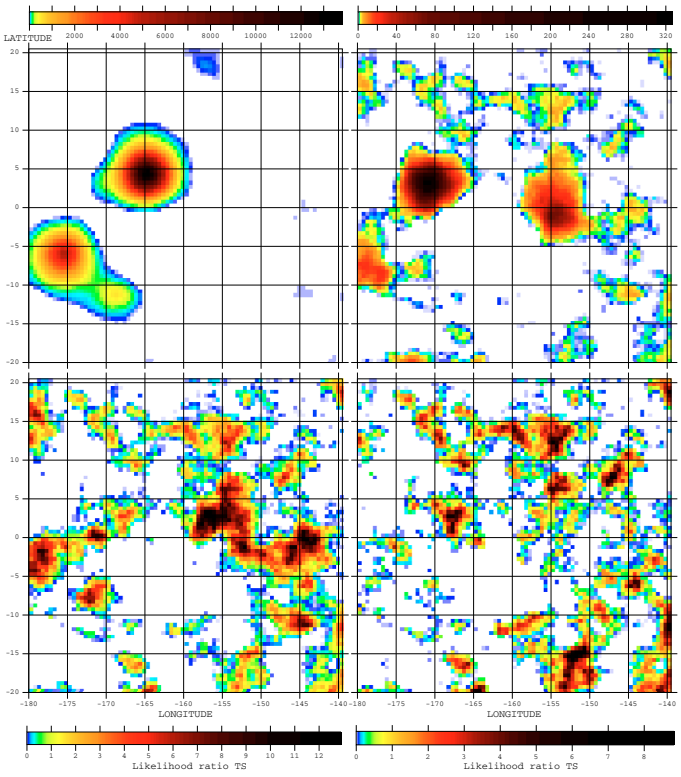

Fig. 3. An example of the iterative source detection with the 2D binned likelihood around Geminga at energies above 100 MeV. 4 consecutive TS maps are shown. Sources are detected, then are included in the background for the next step until no significant one is left. The colourbar gives TS.

deformed projection. Sources detected only once were not included in the list unless their latitude or declination were higher than 40° or their longitude or right ascension were less than 5° from the map edges.

At this stage, most sources have three possible positions (with energy) for a given observation. We chose among the three the position corresponding to the smallest 95% confidence contour, unless its peak $\sqrt{TS}$ was a factor of 1.5 smaller than found in another energy band. The latter condition reduces the risk of incorrect source assignment during the cross-comparison phase. Sources found at low energy, but not at high energy were included in the list, as well as sources found only at high energy.

We used the same criteria to cross-compare the source positions for individual periods and summed cycles to obtain a final list of candidate sources with the most accurately determined position from the different energy bands and periods/cycles. We followed the entire procedure for both the Ring and Galprop interstellar backgrounds. We obtained respectively 1192 and 1225 candidate sources with the Ring and Galprop models. Source fluxes and $\sqrt{TS}$ values above 100 MeV were calculated for these sets of positions for the different periods and cycles. Unlike in 3EG, we did not adjust the position of the identified sources (AGN or pulsars) to that of their radio counterpart.

We adopted the same detection threshold as for the 3EG catalogue ($\sqrt{TS} > 5$ at $|b| < 10°$ and $\sqrt{TS} > 4$ elsewhere) and found 188 and 208 significant sources for the Ring and Galprop models, respectively. We manually checked the TS maps of all sources that barely passed the detection threshold with the Ring model and for which $\sqrt{TS} \sim 3$ with the Galprop one.

We emphasize that the order and criteria applied to cross-correlate positions between the excesses detected in different energy bands and time periods can strongly affect the catalog list close to the detection threshold. Several strategies were tested before adopting the present one, but one must remember that a faint source can pass or drop below the threshold by slightly changing its position or that of its neighbours. Given the steep increase in source numbers with decreasing TS, we emphasize that a small change in the TS threshold, alternatively in the background over which the source TS is calculated, produce a large change in the number of catalogue entries. For instance, lowering the $\sqrt{TS}$ threshold by 0.1 would add 27 sources.

5. Catalogue description

The EGR acronym was adopted for the EGret Revised source list presented in Tables 2 and A.1 in a format similar to the 3EG one. As explained above, the source characteristics (position and flux, and their uncertainties) were determined with the Ring model because of its higher flexibility, better fit, and flatter residual map. A secondary position and flux was measured with the Galprop model and is listed in Tables 2 and A.1 to illustrate the amplitude of the systematic uncertainties due to the choice of interstellar model.

Table 2. The EGR catalogue. The three first sources are shown. The full catalogue is available after the references.

Num	Name	*RA*	Dec	*l*	*b*	θ_{95}	*F*	σ_F	Cnts	$\sqrt{TS}$	*vp*	l_{sys}	b_{sys}	F_{sys}	3EG
1	EGR J0008+7308	2.01	73.14	119.75	10.54	0.20	39.7	4.4	330	10.9	p19	119.75	10.54	41.0	3EGJ0010+7309
							63.9	11.6	96	7.2	p1				
							33.4	9.6	61	4.1	p2				
							22.4	8.7	37	3.0	p4				
							48.8	7.4	162	8.2	p12				
							21.6	7.3	52	3.4	p34				
							37.0	5.3	212	8.5	p1234				
							44.6	8.3	115	6.6	p56				
							33.1	9.7	60	4.0	2110				
2	EGR J0028+0457	7.06	4.95	112.15	–57.44	0.51	14.3	4.6	31	4.1	p34	112.15	–57.44	14.4	
							7.2	4.8	13	1.7	p1				
							13.9	5.9	20	3.0	p3				
							14.0	7.2	10	2.7	p4				
							7.2	4.8	13	1.7	p12				
							10.7	3.3	43	4.0	p1234				
							10.4	3.1	46	4.1	p19				
							24.2	11.1	14	2.9	3200				
							24.7	15.6	6	2.3	3360				
3	EGR J0039-0945	9.75	–9.75	112.76	–72.38	0.27	13.0	3.5	48	4.8	p19	112.65	–72.40	13.1	3EGJ0038-0949
							14.6	5.8	23	3.4	p1				
							15.7	5.4	24	4.0	p4				
							14.6	5.8	23	3.4	p12				
							11.0	4.5	22	3.2	p34				
							12.3	3.6	43	4.5	p1234				
							22.2	17.7	5	1.6	p789				

Sources found within a radius of 1.5 PSF FWHM from a very bright source, and/or with very asymmetric TS map contours are not included in Tables 2 and A.1. We remark, however, that they represent significant excesses of photons above the background that may be due to extended sources, or structures not properly modelled in the interstellar emission, or artifacts due to incorrect PSF tails. This list of 14 confused sources is given in Table B.1, under the acronym EGRc for EGret Revised confused.

For both tables, the description for each column follows:

1. Num: source number in order of increasing right ascension.
2. Name: source name based on J2000 coordinates.
3. *RA* and Dec: J2000 equatorial coordinates in degrees.
4. *l* and *b*: Galactic coordinates in degrees.
5. θ_{95}: angular radius, in degrees, of a circular cone that contains the same solid angle as the 95% confidence contour.
6. *F*: flux in 10^{-8} photon cm^{-2} s^{-1} for $E > 100$ MeV and for each time period.
7. σ_F: 1σ statistical flux uncertainty in 10^{-8} photon cm^{-2} s^{-1}.
8. Cnts: number of photons detected with $E > 100$ MeV.
9. $\sqrt{TS}$: statistical significance of the detection.
10. vp: short viewing period as defined in Table 1 or summed cycles noted p*x* for cycle *x*, *pijkl* for the sum of cycles *i*, *j*, *k*, and *l*, and p19 for the total of 9 cycles.
11. l_{sys} and b_{sys} : Galactic longitude and latitude obtained with the Galprop background model.
12. F_{sys}: flux obtained with the Galprop background model, in 10^{-8} photon cm^{-2} s^{-1}.
13. 3EG: third EGRET catalog counterpart source name if one exists within a radius of 1 PSF FWHM (2° for $E > 100$ MeV) from the EGR source and if the nearest neighbour relation between the EGR and 3EG sources is univocal (the nearest neighbour of the EGR source is the 3EG one and vice versa).

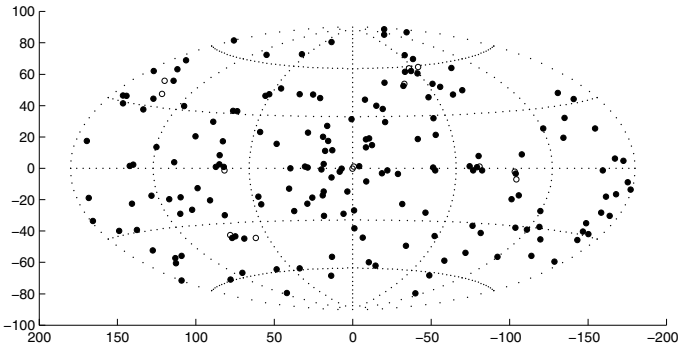

Fig. 4. Spatial distribution, in Galactic coordinates, of the EGR sources. The confused sources are marked as open circles.

6. Comparison with the 3EG catalogue

The revised catalogue contains 174 sources plus 14 confused sources compared to the 265 entries of the 3EG catalogue (excluding the Vela artifacts). Their spatial distribution across the sky looks different from that of the 3EG sources, as illustrated in Figs. 4 and 5. The accumulation of faint 3EG sources within 30° of the Galactic centre is strongly reduced in the new results and fewer sources are seen below 30° in general. These changes at low and mid latitudes are primarily due to the increase in background intensity from new HI, CO, and dark gas structures. At high latitude, the use of more γ-ray observations and of a revised large-scale IC component in the background may also explain why a handful of 3EG sources have fallen below the detection threshold whereas new sources are now detected.

The names of the 107 unconfirmed 3EG sources are listed in Table 3 and they are displayed in Fig. 6. They comprise only six sources firmly identified as AGN by Hartman et al. (1999), but flagged as extended or confused sources by the EGRET team. In fact, the proportion of these extended or confused cases among

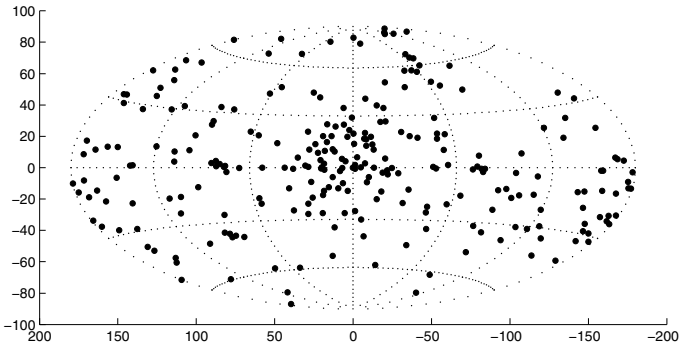

Fig. 5. Spatial distribution, in Galactic coordinates, of the 3EG sources.

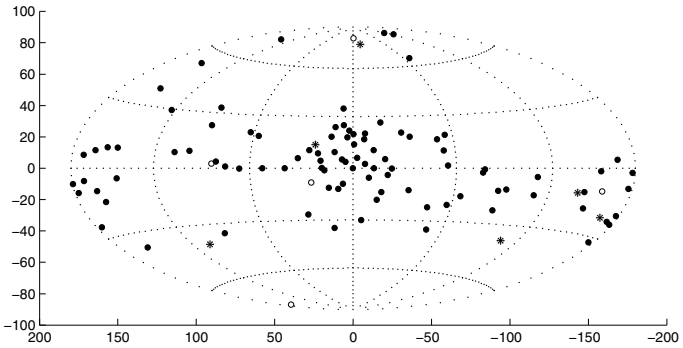

Fig. 6. Spatial distribution, in Galactic coordinates, of the 3EG sources with no counterpart in EGR: the unidentified sources as circles and the identified AGN as stars. The filled circles and stars mark the sources that were flagged as extended or confused in the 3EG catalogue.

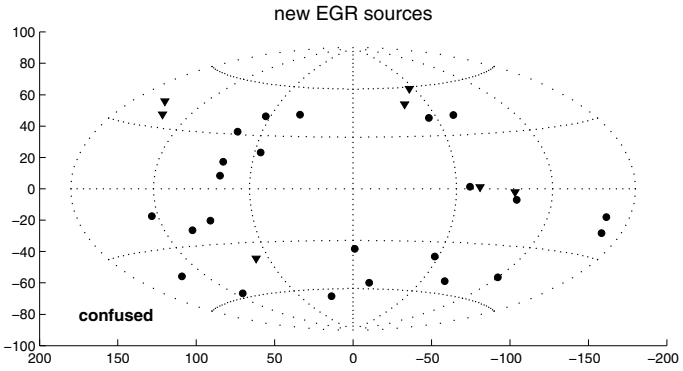

Fig. 7. Spatial distribution, in Galactic coordinates, of the new EGR sources with no 3EG counterpart. The confused sources are marked as open circles.

Table 3. Names of the 3EG sources with no EGR counterpart.

3EG J0130-1758	3EG J0245+1758	3EG J0323+5122
3EG J0348+3510	3EG J0404+0700	3EG J0407+1710
3EG J0416+3650	3EG J0426+1333	3EG J0435+6137
3EG J0439+1555	3EG J0439+1105	3EG J0458-4635
3EG J0459+0544	3EG J0459+3352	3EG J0500+2529
3EG J0510+5545	3EG J0520+2556	3EG J0521+2147
3EG J0533+4751	3EG J0542+2610	3EG J0542-0655
3EG J0546+3948	3EG J0556+0409	3EG J0616-0720
3EG J0622-1139	3EG J0628+1847	3EG J0634+0521
3EG J0702-6212	3EG J0706-3837	3EG J0747-3412
3EG J0808-5344	3EG J0821-5814	3EG J0910+6556
3EG J1013-5915	3EG J1014-5705	3EG J1045-7630
3EG J1052+5718	3EG J1212+2304	3EG J1222+2315
3EG J1227+4302	3EG J1235+0233	3EG J1249-8330
3EG J1300-4406	3EG J1308+8744	3EG J1308-6112
3EG J1316-5244	3EG J1323+2200	3EG J1329+1708
3EG J1329-4602	3EG J1447-3936	3EG J1500-3509
3EG J1527-2358	3EG J1600-0351	3EG J1616-2221
3EG J1627-2419	3EG J1631-1018	3EG J1631-4033
3EG J1633-3216	3EG J1634-1434	3EG J1635-1751
3EG J1639-4702	3EG J1646-0704	3EG J1649-1611
3EG J1653-2133	3EG J1659-6251	3EG J1704-4732
3EG J1709-0828	3EG J1714-3857	3EG J1717-2737
3EG J1718-3313	3EG J1720-7820	3EG J1733+6017
3EG J1735-1500	3EG J1741-2050	3EG J1741-2312
3EG J1744-0310	3EG J1744-3011	3EG J1744-3934
3EG J1757-0711	3EG J1800-0146	3EG J1806-5005
3EG J1810-1032	3EG J1823-1314	3EG J1824+3441
3EG J1824-1514	3EG J1825+2854	3EG J1828+0142
3EG J1834-2803	3EG J1836-4933	3EG J1850+5903
3EG J1850-2652	3EG J1858-2137	3EG J1903+0550
3EG J1904-1124	3EG J1928+1733	3EG J1958+2909
3EG J1958-4443	3EG J2016+3657	3EG J2020-1545
3EG J2022+4317	3EG J2034-3110	3EG J2035+4441
3EG J2100+6012	3EG J2206+6602	3EG J2219-7941
3EG J2255+1943	3EG J2359+2041	

Table 4. Names of the new EGR sources with no 3EG counterpart.

EGR J0028+0457	EGR J0057-7839	EGR J0100+4927
EGR J0141+1719	EGR J0243-5930	EGR J0413-3742
EGR J0509+0550	EGR J0540+0657	EGR J1122-5946
EGR J1158-1950	EGR J1259-2209	EGR J1619+2223
EGR J1642+3940	EGR J1740+4946	EGR J1814+2932
EGR J1920+4625	EGR J1959+4322	EGR J2027-4206
EGR J2202+3340	EGR J2233-4812	EGR J2258-2745
EGR J2308+3645	EGRc J0818-4613	EGRc J0842-4501
EGRc J0912+7146	EGRc J0927+6054	EGRc J1038-5724
EGRc J1255-0404	EGRc J1332-1217	EGRc J2215+0653

the unconfirmed 3EG sources is overwhelming (95%) and significantly larger than among the confirmed ones. The unconfirmed and confirmed 3EG groups show 69% and 33% of possibly extended 'em' sources respectively. Figure 6 also shows that the vast majority of unconfirmed 3EG sources were unidentified and spatially correlated with the Gould Belt system of nearby clouds. They follow the characteristic trace of the inclined Belt across the sky, gathering at $|b| < 30°$, more at positive latitudes toward the Galactic centre, and below the plane at the anticentre. The EGR source sky distribution in Fig. 4 does not exhibit the Gould Belt signature anymore.

The fact that many 3EG sources are unconfirmed by the present analyses should not cast doubts on the detection method from a statistical point of view. They did correspond to significant photon excesses above the background in the 3EG analyses, but, in the absence of some structures in the predicted interstellar background, an ensemble of point sources with the wide EGRET PSF would compensate for the missing clouds and yield an excellent fit to the data. Figure 8 illustrates this fact for the unidentified source 3EG J0556+0409 detected at 7.2σ in 3EG. The left side shows the TS-map corresponding to the second stage of the iterative source detection around Geminga above 100 MeV. It is the same as in Fig. 3 but we have used here the 3EG diffuse emission model instead of the Ring one. The same sources are detected apart from 3EG J0556+0409, which is not seen in Fig. 3. Instead an excess of diffuse emission appears in the ratio of the Ring to 3EG background intensities (Fig. 8,

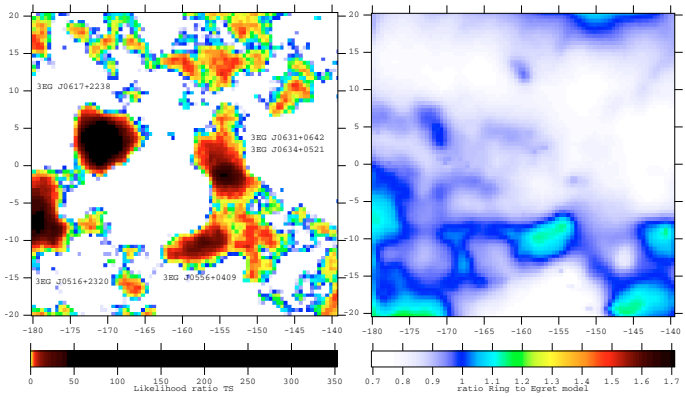

Fig. 8. Second stage of the iterative source detection around Geminga (see Fig. 3) obtained using the 3EG model (*left*) and map of the Ring model intensity divided by the 3EG one (*right*). The excess in the TS map assigned in 3EG to the 3EG J0556+0409 point source corresponds to a local underestimation of the diffuse emission in the 3EG model. Maps are given in 0.5° bins and galactic coordinates.

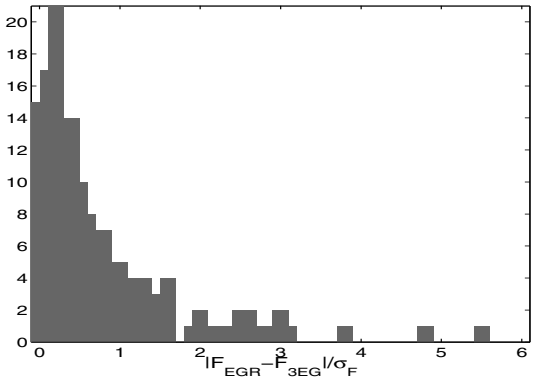

Fig. 9. Histogram of the relative flux differences $|F_{\rm EGR} - F_{\rm 3EG}|/\sigma_{F_{\rm EGR}}$ measured between the EGR and 3EG counterparts in units of the statistical error on flux for each source. All fluxes are measured above 100 MeV.

right). *The photons attributed to a point source in 3EG in fact originate in a gas cloud within the Galaxy.* This is probably still the case in the present analysis, although to a lesser degree, in particular at very low latitude where the optical thicknesses in HI and CO severely limit our knowledge of the true column densities. Other sources may also be due to increased cosmic-ray densities in specific clouds with respect to the local Galactic average. Over-irradiated clouds close to cosmic-ray sources would be detected as a single or cluster of point sources, depending on their angular scale.

For the 81 EGR sources that do have a 3EG counterpart, we find reasonable agreement in position and flux from both analyses. On average, we find 3% lower fluxes in the EGR analysis with respect to the 3EG one because of the increase in Galactic background. Figure 9 shows the histogram of ratios of the EGR and 3EG flux difference over the statistical error in flux for each source: $|F_{\rm EGR} - F_{\rm 3EG}|/\sigma_{F_{\rm EGR}}$. We considered the EGR flux for the observation with the highest $\sqrt{TS}$ and compared it with the 3EG counterpart flux for the same time period if available. Average P19 fluxes were compared to the 3EG P1234 average for non flaring sources. The flux differences are modest (17% rms dispersion) and in most cases smaller than the statistical

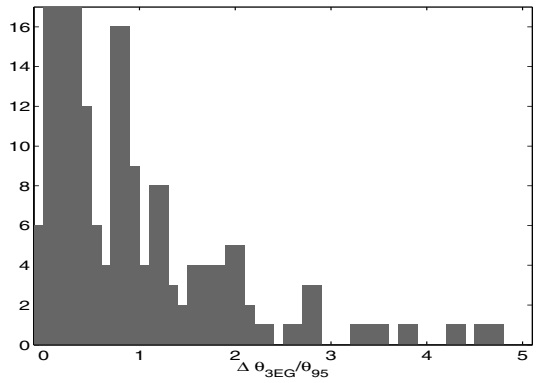

Fig. 10. Histogram of the relative angular separation between the positions found for the EGR and 3EG counterparts in units of the 95% confidence angle for each source.

uncertainties on flux estimates. Similarly, Fig. 10 indicates that the angular separations between EGR and 3EG counterparts are often consistent with the θ_{95} error radii. Thirty sources were, however, found as distant as 0.5° from the 3EG position. This will have a large impact on counterpart searches and identification at other wavelengths.

On the other hand, we find 30 new EGR sources with no 3EG counterpart. Their names are listed in Table 4 and they are displayed in Fig. 7. Most are detected just above the threshold and 11 were indeed present in the 3EG complementary list, just below the significance threshold.

7. EGR source distributions and potential counterparts

Because of the new gas data that we used at intermediate latitude, the comparison between the EGR and 3EG source characteristics enables us to judge, to some extent, the impact of our limited knowledge of gas mass tracers. The comparison between the flux and positions obtained with the Ring and Galprop models enables us to estimate the systematic uncertainties due to our limited knowledge of the true cosmic-ray distribution across the Galaxy. Figures 11 and 12 indicate that, in most cases, the differences are smaller than the statistical uncertainties. The distribution of 95% confidence radii peaks between ~0.2° and ~0.7°. The uncertainty in the background creates an additional systematic error of ~0.2° for most sources, which should be kept in mind while searching for counterpart sources.

We searched the EGR error circles for potential counterparts of interest such as pulsars from the ATNF catalogue (Manchester et al. 2005), blazar candidates from the ASDC list (Massaro et al. 2005) and the CGRaBS list (Healey et al. 2008), other flat radiosources from the CRATES compilation (Healey et al. 2007), supernova remnants from the Green catalogue (Green 2006), OB associations (Mel'Nik & Efremov 1995), and X-ray and TeV pulsar wind nebulae (Li et al. 2008 and Grenier 2008). The results are displayed in Fig. 13. We have found 13 radio pulsar associations in addition to the 6 objects firmly identified by EGRET. Thirteen EGR sources coincide with supernova remnants, 9 with pulsar wind nebulae, 7 with OB associations, 53 with blazar candidates, and 19 with other flat radiosources. These associations should not be considered as source identifications, but as spatial coincidences worthy of further investigation, in particular with the improved angular resolution of GLAST. Yet, they reveal that as many as 87 sources have no obvious counterpart among the well-known γ-ray emitters, despite the

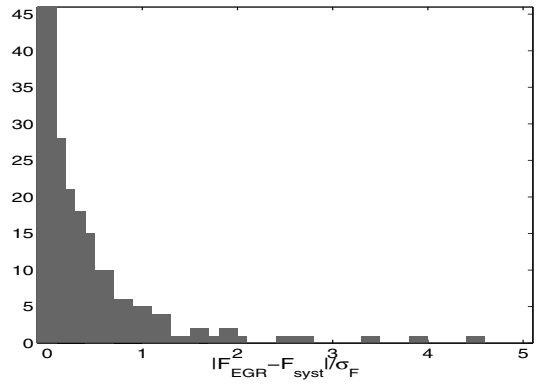

Fig. 11. Histogram of the relative flux differences $|F_{\rm EGR} - F_{\rm sys}|/\sigma_{F_{\rm EGR}}$ measured with the Ring and Galprop models in units of the statistical error in flux for each source. All fluxes are measured above 100 MeV.

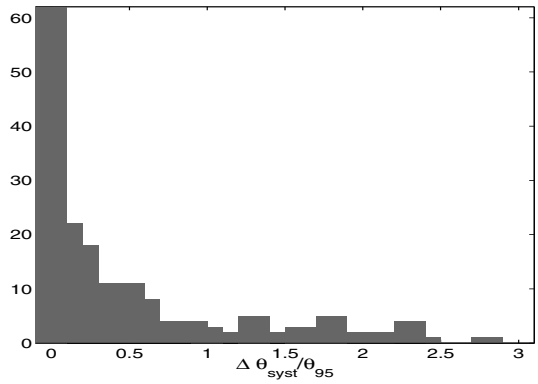

Fig. 12. Histogram of the relative angular separation between the positions found with the Ring and Galprop models in units of the 95% confidence angle for each source.

large number of pulsars (1775) and radiosources (11 000) that were cross-correlated with sources and spread across the entire sky and along the Galactic plane. The lack of blazar counterparts is all the more surprising because the spatial distribution of sources off the plane is reminiscent of an isotropic, therefore extragalactic, distribution. The latitude distribution, shown in Fig. 14, is consistent above 30° with a sample drawn from a uniform population, according to the exposure map, as shown by the black curve. The distribution flattens at lower latitude because of the increased background that drastically limits the survey sensitivity. Studying the consistency with an extragalactic population at medium latitudes and the implication of the lack of flat radio sources is beyond the scope of this paper and will be addressed in a future work. The sharp peak below 3° in latitude indicates young emitters. Their clustering in the inner Galaxy ($l \leq 30°$), toward the direction tangent to the Carina arm, and toward the Cygnus region outlines their close relationship to large molecular complexes and star forming regions at a distance of a few kpc.

8. Discussion on specific sources

There is considerable interest in the physical processes occurring in the Galactic centre region. The 3EG catalogue lists one source located toward the Galactic centre, 3EG J1744-3011. We find two point sources in this region, EGR J1740-2851 at $l = -0.55°$, $b = 1.05°$ and EGR J1747-2852 at $l = 0.21°$, $b = -0.24°$. Figure 15 displays the TS-map for photons of energies that are higher than 1 GeV above the 3EG and the Ring background models. The θ_{95} error radius around EGR J1740-2851 and EGR J1747-2852 formerly excludes the Galactic Centre, but source locations and fluxes in this direction should be interpreted with extreme caution since the high gas optical depth around the Galactic centre and the velocity pile-up toward the centre induce large uncertainties in the total gas column densities.

Coincidences with supernova remnants were noted (Sturner & Dermer 1995) and are confirmed in the present analysis (see Table 5), but several also host a pulsar wind nebula, as in CTA 1 and IC 443; we therefore require far higher resolution γ-ray images to identify the origin of the emission, especially in these crowded regions. EGRET detections are confirmed toward two TeV-emitting wind nebulae around PSR J1420-6048 (in Kookaburra, EGRJ1418-6040) and PSR J1826-1334 (EGRJ1825-1325). Another interesting candidate is the wind nebula of the 11 kyr old and very energetic pulsar PSR J2229+6114 toward EGRJ2227+6114.

We note, as shown in Fig. 16, the positional coincidence within 0.5° between the new EGR J0028+0457 source and the millisecond X-ray pulsar PSR J0030+0451. This 300 pc distant pulsar, discovered in 2000 (Somer 2000, D'Amico 2000), has an X-ray counterpart exhibiting a double peaked pulse profile as measured by ROSAT (Becker et al. 2000). Millisecond pulsars have low magnetic fields and produce relatively few electron-positron pairs; the electric field is not therefore screened and the spectral cutoff due to pair production attenuation occurs at high energy. They are good candidates for accelerating particles to high energies. Harding et al. (2005) predicted a γ-ray flux for PSR J0030+0451 well above that of the γ-ray millisecond pulsar PSR J0218+4232 for which a pulsed emission was marginally detected (Kuiper et al. 2000).

Four massive binaries were detected at TeV energies, namely PSR B1259-63 (Aharonian et al. 2005), LSI +61° 303 (Albert et al. 2006), LS 5039 (Aharonian et al. 2006), and Cyg X-1 (Albert et al. 2007), which illustrates the very efficient particle acceleration in compressed or shocked pulsar winds, as well as in microquasar jets. Inverse Compton scattering of the bright stellar radiation would dominate at GeV energies. We find no interesting EGRET counterpart to these high-energy objects, besides the LSI +61° 303 radiosource. The latter has long been associated with the COS-B source 2CG 135+01 and the EGRET source 2EG J0241+6119 (Kniffen et al. 1997), yet has moved out of the 3EG error box and the marginal γ-ray variability could not be associated with radio flux variations. In the present analysis, we find the radiosource very close to the centre of the EGR J0240+6112 source. On the other hand, we find no source toward the dust enshrouded microquasar candidate, AX J1639.0-4642, or the Be/X-ray binary, AO 0535+26, both proposed as 3EG counterparts (Combi et al. 2003; Romero et al. 2001).

Another noticeable new source is EGR J1642+3940 detected at 5.8σ rather close to 3C345. 3C345 is one of the most prominent flat spectrum ($\alpha = -0.1$) radio-loud, superluminal sources and is therefore an excellent candidate to be a γ-ray blazar. EGRET surveyed this region 12 times, in particular during period 5190 when a flare was found. We analyzed this particular period using the Ring model since it had not been used in the overall detection search. Figure 17 shows the resulting TS contour, for photons of energies above 100 MeV, that is well centered on 3C345. The cross corresponds to the EGR position (period 5190), the plus sign to the position with maximum likelihood, and the black dots to both the position of 3C345 and a nearby AGN. A marginal detection was also achieved for period 3034 at a level of 2.1σ. It should be noted, however, that the small photon excess above 500 MeV was attributed to a flare

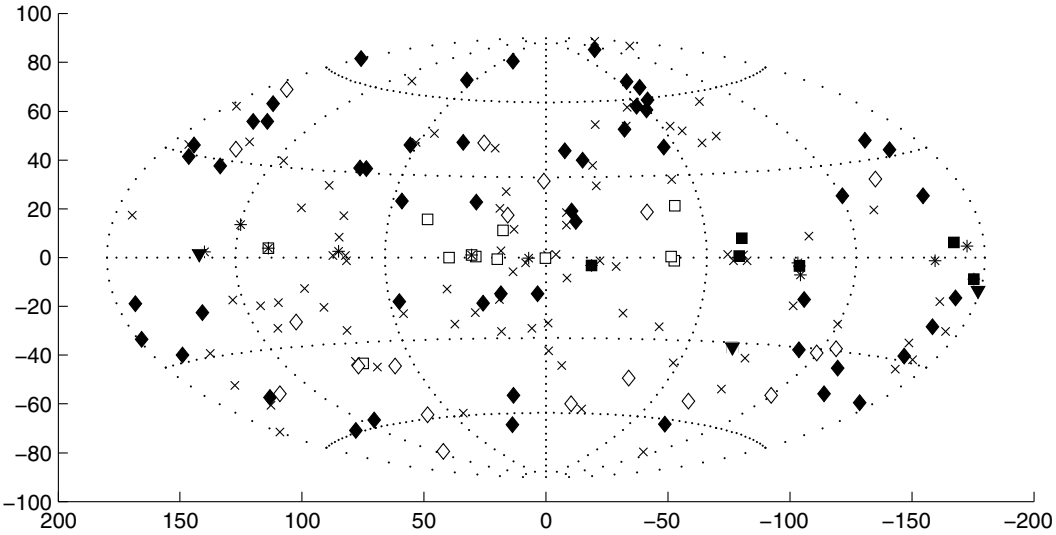

Fig. 13. The revised EGRET source catalog, shown in Galactic coordinates. The symbols indicate the counterpart types found in the error box: identified pulsars as black squares; other ATNF pulsars as open squares; LSI +61 303, LMC, and solar flare as black triangles; ASDC and CGRaBS blazar candidates as black diamonds; other flat-spectrum radiosources from CRATES as open diamonds; supernova remnants from the Green catalogue as stars; no counterpart as crosses.

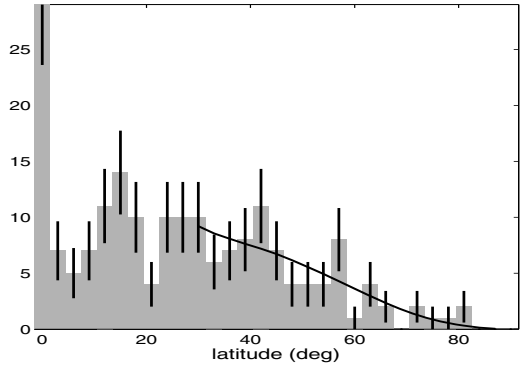

Fig. 14. Latitude distribution of the EGR sources with young Galactic sources at $|b| < 3°$, nearly isotropically distributed sources far from the plane, as expected from the black curve, and a flattening at mid-latitude because of the rapid increase in the interstellar background flux.

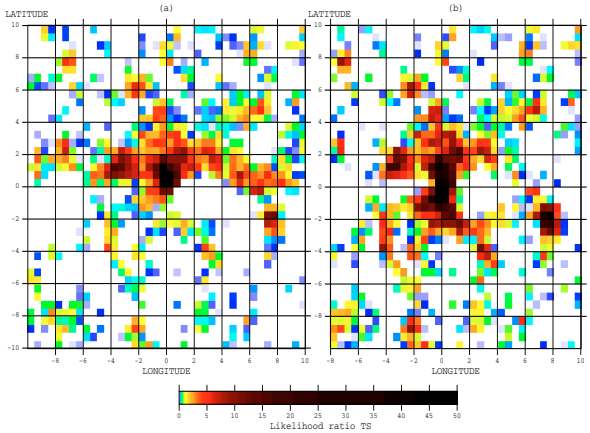

Fig. 15. TS-map obtained at energies above 1 GeV toward the Galactic centre above the 3EG **a)** and Ring **b)** interstellar model

from Mrk 501 by Kataoka et al. (1999) because the centroid was closer to the famous TeV source, so the association of EGR J1642+3940 with 3C345 is unclear. GLAST should easily confirm or disprove the association.

Several radiogalaxies (Cen A, NGC 6251, J1737-15) and a Seyfert 1 galaxy (GRS 1734-292) have been proposed as possible counterparts to 3EG sources (Hartman et al. 1999; Combi et al. 2003; Foschini et al. 2005; Di Cocco et al. 2004). These objects triggered some interest because their identification would raise important questions about the origin of the γ rays at large angles from the strongly beamed emission from the jet. We do not, however, confirm the spatial coincidence with EGR sources in the present work. All these galaxies are located well beyond the 95% confidence region of EGR sources.

Table 5. Names of the sources and supernova remnants found in spatial coincidence.

EGRJ0008+7308	G119.5+10.2	CTA1
EGRJ0617+2238	G189.1+3.0	IC443
EGRJ0633+0646	G205.5+0.5	Monoceros
EGRJ1710-4435	G343.0-6.0	RCW114
EGRJ1800-2328	G6.4-0.1	W28
EGRJ1800-2328	G6.5-0.4	
EGRJ1838-0420	G27.8+0.6	
EGRJ1838-0420	G28.8+1.5	
EGRJ2020+4019	G78.2+2.1	γ Cygni
EGRJ2227+6114	G106.3+2.7	
EGRJ0225+6240	G132.7+1.3	HB3

9. Conclusions

We have searched for point-like sources in the reprocessed EGRET data from cycle 1 to 9 using new interstellar background models based on the most recent HI, CO, and dark gas data, as well as two different assumptions for the cosmic-ray distribution (the GALPROP diffusion model or a radial emissivity gradient fitted to the diffuse EGRET data). We have used the 3EG tools, likelihood method, procedure, and significance threshold to detect sources, but have expanded the search to 3 different energy bands (above 100 MeV, 0.3–1 GeV, and above 1 GeV). The resulting number of detected sources has decreased by more than a third. Many unidentified sources, in particular among those spatially associated with the Gould Belt, are not confirmed as significant excesses. Their emission can be explained by the additional interstellar emission and its structure. Several interesting

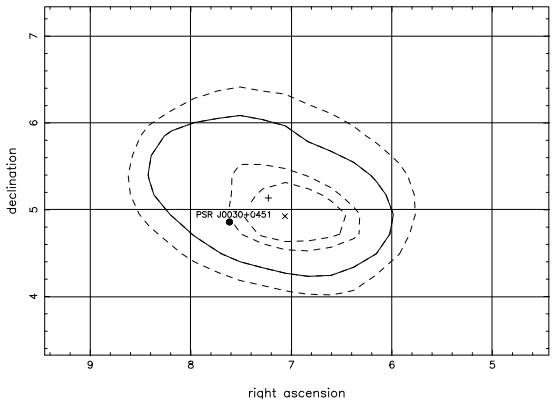

Fig. 16. Likelihood TS contours for energies above 100 MeV and periods incompassing PSR J0030+0451. The cross, the plus sign and the black dot respectively mark the EGR catalog position, the position with maximum likelihood and the pulsar location.

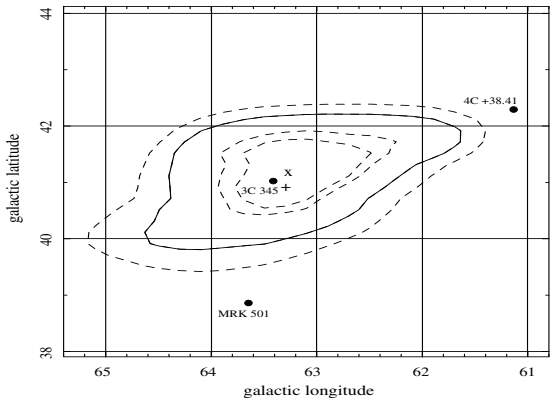

Fig. 17. Likelihood TS contours (50%, 68%, 95% and 99% confidence) for energies above 100 MeV and period 5190. The cross is the EGR catalog position, the plus sign the position with maximum likelihood and the black dots mark the radio positions of 3C345, Mrk 501, and 4C+38.41.

counterparts to 3EG sources, such as radiogalaxies, massive binaries, and microquasars, are now found outside the 95% confidence region. We have cross-correlated the new source positions with large pulsar, supernova remant, pulsar wind nebulae, OB associations, and radiosource catalogues, yet half the sample has no attractive counterpart among the potential γ-ray emitters. Thirty new possible γ-ray sources have also been found.

This EGR catalog will be available in FITS format at the Strasbourg astronomical Data Center (CDS) and in ASCII format at http://www.aim.univ-paris7.fr/EGRET_catalogue/home.html

Acknowledgements. We are deeply grateful to Bob Hartman for his helpful explanations about the construction of the 3EG catalogue, and to Seth Digel and Andy Strong for their help with the gas and Galprop maps.

References

Aharonian, F., Akhperjanian, A. G., Aye, K.-M., et al. 2005, A&A, 442, 1
Aharonian, F., Akhperjanian, A. G., Bazer-Bachi, A. R., et al. 2006, A&A, 460, 743
Albert, J., Aliu, E., Anderhub, H., et al. 2006, Science, 312, 1771
Albert, J., Aliu, E., Anderhub, H., et al. 2007, ApJ, 665, L51
Becker, W., Trumper J., Lommen, A. N., & Backer, D. C. 2000, ApJ, 545, 1015
Bertin, E., & Arnouts, S. 1996, A&AS, 117, 393
Combi, J. A., Romero, G. E., Paredes, J. M., Torres, D. F., & Ribó, M. 2003, ApJ, 588, 731
Combi, J. A., Ribó, M., Mirabel, I. F., & Sugizaki, M. 2004, A&A, 422, 1031
Dame, T. M., Hartmann, D., & Thaddeus, P. 2001, ApJ, 547, 792
D'Amico, N. 2000, in Pulsar Astronomy - 2000 and Beyond, ed. M. Kramer, N. Wex, & R. Wielebinski (San Francisco: ASP), 202th ASP Conf. Ser., 27
Di Cocco, G., Foschini, L., Grandi, P., et al. 2004, A&A, 425, 89
Fichtel, C. E., Bertsch, D. L., Chiang, J., Chiaberge, M., Grandi, P., et al. 1994, ApJS, 94, 551
Finkbeiner, D. P., Davis, M., & Schlegel, D. J. 1999, ApJ, 524, 867
Foschini, L., et al. 2005, A&A, 433, 515
Gehrels, N., Macomb, D. J., Bertsch, D. L., Thompson, D. J., & Hartman, R. C. 2000, Nature, 404, 363
Green D. A. 2006, A Catalogue of Galactic Supernova Remnants (2006 April version), Astrophysics Group, Cavendish Laboratory (UR: Cambridge)
Grenier, I. A. 1995, Adv. Space Res., 15, 73
Grenier, I. A. 2000, A&A, 364, L93
Grenier, I. A. 2004, Cosmic Gamma-Ray Sources, 304, 47
Grenier, I. A., Casandjian, J.-M., & Terrier, R. 2005, Science, 307, 1292
Grenier, I. A. 2008, 30th ICRC, Merida, Mexico, in press
Harding, A. K., Usov, V. V., & Muslimov, A. G. 2005, ApJ, 622, 531
Hartman, R. C., Bertsch, D. L., Bloom, S. D., et al. 1999, ApJS, 123, 79
Healey, S. E., et al. accepted for publication in ApJS
Healey, S. E., Romani, R. W., Taylor, G. B., et al. 2007, ApJS., 171, 61-71
Hermsen, W., Kuiper, L., Verbunt, F., et al. 2000, Proc. fifth Compton Symp., 510, 257
Hunter, S. D., Bertsch, D. L., Catelli, J. R., et al. 1997, ApJ, 481, 205
Kalberla, P. M. W., Burton, W. B., Hartmann, D., et al. 2005, A&A, 440, 775
Kataoka, J., Mattox, J. R., Quinn, J., et al. 1999, Astroparticle Physics, 11, 149
Kniffen, D. A., Alberts, W. C. K., Bertsch, D. L., et al. 1997, ApJ, 486, 126
Kuiper, L., Hermsen, W., Verbunt, F., et al. 2000, A&A, 359, 615
Lagache, G. 2003, A&A, 405, 813
Lamb, R. C., & Macomb, D. J. 1997, ApJ, 488, 872
Li, X.-H., Lu, F.-J., Li, Z., 2007 [arXiv:0707.4279v1]
Massaro, E., Sclavi, S., Giommi, P., Perri, M., & Piranomonte, S. 2005, Multifrequency Catalogue of Blazars, Vol. I, Aracne ed-itrice, Roma
Mattox, J. R., Bertsch, D. L., Chiang, J., et al. 1996, ApJ, 461, 396
Manchester, R. N., Hobbs, G. B., Teoh, A. & Hobbs, M. 2005, M., Astron. J., 129, 1993
Mel'Nik, A. M., & Efremov, Y. N. 1995, Astron. Lett., 21, 10
Moskalenko, I. V., Porter, T. A., & Strong, A. W. 2006, ApJ, 640, L155
Nolan, P. L., Tompkins, W. F., Grenier, I. A., & Michelson, P. F. 2003, ApJ, 597, 615
Perrot, C. A., & Grenier, I. A. 2003, A&A, 404, 519
Pollock, A. M. T., Masnou, J. L., Bignami, G. F., et al. 1981, A&A, 94, 116
Porter, T. A., et al. 2005, International Cosmic Ray Conference, 4, 77
Romero, G. E., Kaufman Bernadó, M. M., Combi, J. A., & Torres, D. F. 2001, A&A, 376, 599
Schlegel, D. J., Finkbeiner, D. P., & Davis, M. 1998, ApJ, 500, 525
Somer, A. 2000, in Pulsar Astronomy - 2000 and Beyond, ed. M. Kramer, N. Wex, & R. Wielebinski (San Francisco: ASP), 202th ASP Conf. Ser., 17
Sowards-Emmerd, D., Romani, R. W., Michelson, P. F., Healey, S. E., & Nolan, P. L. 2005, ApJ, 626, 95
Sreekumar, P., Bertsch, D. L., Dingus, B. L., et al. 1998, ApJ, 494, 523
Strong, A. W., & Mattox, J. R. 1996, A&A, 308, L21
Strong, A. W., Bloemen, J. B. G. M., Dame, T. M., et al. 1988, A&A, 207, 1
Strong, A. W., Moskalenko, I. V., & Reimer, O. 2004a, ApJ, 613, 962
Strong, A. W., Moskalenko, I. V., Reimer, O., Digel, S., & Diehl, R. 2004b, A&A, 422, L47
Strong, A. W., Moskalenko, I. V., & Ptuskin, V. S. 2007, Ann. Rev. Nucl. Particle Sci., 57, 285
Sturner, S. J., & Dermer, C. D. 1995, A&A, 293, L17
Thompson, D. J., Bertsch, D. L., Dingus, B. L., et al. 1995, ApJS, 101, 259
Thompson, D. J., Bertsch, D. L., Dingus, B. L., et al. 1996, ApJS, 107, 227

Table A.1. The EGR catalogue.

Num	Name	*RA*	Dec	*l*	*b*	θ_{95}	*F*	σ_F	Cnts	$\sqrt{TS}$	*vp*	$l_{\rm sys}$	$b_{\rm sys}$	$F_{\rm sys}$	3EG
1	EGR J0008+7308	2.01	73.14	119.75	10.54	0.20	39.7	4.4	330	10.9	p19	119.75	10.54	41.0	3EGJ0010+7309
							63.9	11.6	96	7.2	p1				
							33.4	9.6	61	4.1	p2				
							22.4	8.7	37	3.0	p4				
							48.8	7.4	162	8.2	p12				
							21.6	7.3	52	3.4	p34				
							37.0	5.3	212	8.5	p1234				
							44.6	8.3	115	6.6	p56				
							33.1	9.7	60	4.0	2110				
2	EGR J0028+0457	7.06	4.95	112.15	−57.44	0.51	14.3	4.6	31	4.1	p34	112.15	−57.44	14.4	
							7.2	4.8	13	1.7	p1				
							13.9	5.9	20	3.0	p3				
							14.0	7.2	10	2.7	p4				
							7.2	4.8	13	1.7	p12				
							10.7	3.3	43	4.0	p1234				
							10.4	3.1	46	4.1	p19				
							24.2	11.1	14	2.9	3200				
							24.7	15.6	6	2.3	3360				
3	EGR J0039-0945	9.75	−9.75	112.76	−72.38	0.27	13.0	3.5	48	4.8	p19	112.65	−72.40	13.1	3EGJ0038-0949
							14.6	5.8	23	3.4	p1				
							15.7	5.4	24	4.0	p4				
							14.6	5.8	23	3.4	p12				
							11.0	4.5	22	3.2	p34				
							12.3	3.6	43	4.5	p1234				
							22.2	17.7	5	1.6	p789				
4	EGR J0057-7839	14.46	−78.65	−57.47	−38.47	0.53	10.5	2.7	73	4.6	p12	−57.46	−38.44	10.3	
							11.5	3.3	56	4.1	p1				
							8.4	4.6	18	2.1	p2				
							9.6	2.5	78	4.5	p1234				
							9.1	2.4	74	4.3	p19				
5	EGR J0100+4927	15.01	49.45	124.37	−13.40	0.27	21.5	6.1	49	4.4	p1	123.94	−14.77	12.9	
							16.2	8.3	21	2.3	p3				
							10.0	9.3	8	1.2	p4				
							12.5	3.9	62	3.7	p12				
							13.7	6.2	29	2.5	p34				
							12.4	3.3	87	4.4	p1234				
							26.4	22.7	6	1.4	p789				
							12.4	3.2	90	4.4	p19				
6	EGR J0117+0254	19.41	2.91	135.83	−59.30	1.15	21.2	5.9	37	4.6	210	135.83	−59.30	21.1	3EGJ0118+0248
							14.0	4.5	39	3.8	p1				
							14.0	4.5	39	3.8	p12				
							5.7	2.7	29	2.3	p1234				
							5.3	2.6	31	2.3	p19				
7	EGR J0141+1719	25.47	17.32	139.75	−43.90	0.85	18.8	5.5	36	4.4	3170	139.52	−43.91	18.4	
							8.8	4.5	24	2.2	p1				
							15.6	5.2	30	3.8	p3				
							8.7	4.4	23	2.2	p12				
							11.0	3.7	36	3.6	p34				
							9.3	2.8	56	3.8	p1234				
							7.1	2.6	46	3.1	p19				
							15.3	6.6	23	2.7	210				
							18.3	14.8	6	1.4	260				
8	EGR J0159-3609	29.78	−36.16	−110.71	−73.04	0.59	12.8	3.7	39	4.6	p1	−110.85	−73.02	12.9	3EGJ0159-3603
							4.6	3.7	9	1.5	p4				
							12.4	3.6	38	4.5	p12				
							9.5	2.7	47	4.5	p1234				
							34.0	26.3	5	1.7	p789				
							8.7	2.5	47	4.3	p19				
9	EGR J0204+1505	31.00	15.09	147.75	−44.26	0.48	25.9	5.7	68	5.8	p1	147.75	−44.27	25.8	3EGJ0204+1458
							3.6	3.5	9	1.1	p3				
							25.7	5.7	67	5.8	p12				
							11.4	2.9	72	4.7	p1234				
							10.0	2.7	70	4.4	p19				
							27.5	6.5	58	5.5	210				
							54.6	25.6	11	3.0	260				
							4.6	3.7	11	1.4	3170				

Table A.1. continued.

Num	Name	*RA*	Dec	l	b	θ_{95}	F	σ_F	Cnts	$\sqrt{TS}$	*vp*	l_{sys}	b_{sys}	F_{sys}	3EG
10	EGR J0210-5058	32.58	−50.97	−83.84	−61.86	0.14	85.1	4.1	840	31.5	p19	−83.82	-61.86	89.7	3EGJ0210-5055
							83.3	6.6	320	18.9	p1				
							44.1	10.6	48	5.7	p2				
							92.7	11.6	119	12.2	p3				
							66.9	9.4	109	10.3	p4				
							75.2	5.6	371	19.5	p12				
							84.7	7.4	247	17.6	p34				
							77.8	4.5	610	25.9	p1234				
							139.9	12.7	202	17.7	p56				
							30.8	12.1	18	3.4	p789				
11	EGR J0216+1128	34.04	11.48	153.74	−46.26	0.98	17.2	4.9	48	4.3	210	153.76	−46.29	17.2	3EGJ0215+1123
							15.7	4.8	44	3.9	p1				
							15.6	4.8	44	3.9	p12				
							4.7	2.4	31	2.1	p1234				
							4.4	2.3	33	2.1	p19				
12	EGR J0223+4300	35.80	43.01	140.25	−16.75	0.21	20.5	2.8	207	9.2	p19	140.25	−16.75	21.3	3EGJ0222+4253
							13.9	4.0	58	4.1	p1				
							13.2	6.8	22	2.3	p2				
							23.4	5.7	61	5.3	p3				
							19.3	9.3	16	2.6	p4				
							14.8	3.5	86	5.0	p12				
							24.9	5.0	85	6.5	p34				
							18.6	2.9	172	8.0	p1234				
							32.7	10.8	27	4.0	p789				
							13.5	6.8	22	2.3	2110				
13	EGR J0238+1659	39.61	16.99	156.47	−38.81	0.34	79.6	9.0	169	12.7	210	156.40	−38.78	82.6	3EGJ0237+1635
							52.6	6.2	184	11.6	p1				
							15.6	5.1	39	3.8	p3				
							10.0	6.4	11	1.8	p4				
							52.3	6.2	183	11.5	p12				
							14.0	4.0	50	4.3	p34				
							32.0	3.7	227	11.3	p1234				
							29.7	3.5	230	11.1	p19				
							13.8	4.8	34	3.6	3170				
14	EGR J0240+2812	40.03	28.20	150.28	−28.84	0.55	11.8	2.4	116	5.7	p19	150.26	−28.83	10.9	3EGJ0239+2815
							13.7	3.5	66	4.7	p1				
							7.9	4.1	25	2.2	p3				
							13.7	7.5	16	2.1	p4				
							13.2	3.5	64	4.6	p12				
							9.4	3.6	40	3.0	p34				
							11.9	2.5	109	5.6	p1234				
							20.1	12.8	9	1.9	p789				
							33.7	11.9	26	3.6	210				
							21.7	12.7	9	2.4	36+				
							11.1	5.9	18	2.2	3170				
15	EGR J0240+6112	40.12	61.20	135.68	1.06	0.12	81.9	5.4	1000	18.2	p19	135.57	1.15	85.5	3EGJ0241+6103
							79.4	10.2	263	9.3	p1				
							121.0	13.4	287	11.4	p2				
							59.9	10.5	179	6.7	p3				
							81.9	15.7	117	6.3	p4				
							97.5	8.2	554	14.7	p12				
							68.2	8.7	301	9.2	p34				
							85.1	6.0	859	17.2	p1234				
							62.6	12.4	132	5.8	p56				
							121.2	13.4	288	11.4	2110				
16	EGR J0243-5930	40.94	−59.50	−80.08	−52.32	0.95	18.6	6.0	31	4.1	p3	−80.41	−52.25	18.1	
							9.2	3.4	31	3.3	p34				
							2.4	1.5	27	1.7	p1234				
							2.4	1.4	30	1.8	p19				
17	EGR J0253-0336	43.25	−3.61	179.25	−52.65	0.60	16.6	5.5	28	4.0	p3	179.08	−52.55	15.5	3EGJ0253-0345
							14.3	4.9	29	3.8	p34				
							3.0	2.1	17	1.6	p1234				
							2.3	2.0	14	1.3	p19				
							16.4	5.5	27	3.9	3170				
18	EGR J0328+2147	52.17	21.79	164.73	−28.04	0.48	16.1	4.9	44	4.1	p3	164.79	−28.00	16.4	3EGJ0329+2149
							13.7	4.0	51	4.1	p34				
							6.2	2.5	58	2.8	p1234				
							21.5	11.0	17	2.4	p789				
							7.3	2.4	75	3.4	p19				
							15.6	6.9	22	2.8	3170				

Table A.1. continued.

Num	Name	*RA*	Dec	l	b	θ_{95}	F	σ_F	Cnts	$\sqrt{TS}$	*vp*	l_{sys}	b_{sys}	F_{sys}	3EG
19	EGR J0338-0203	54.73	−2.06	−171.80	−42.74	0.36	90.7	18.1	61	8.0	p4	−171.74	−42.73	87.7	3EGJ0340-0201
							5.3	3.6	17	1.6	p1				
							12.3	7.3	13	2.0	p3				
							5.4	3.6	18	1.6	p12				
							41.6	7.7	71	7.6	p34				
							18.1	3.6	90	6.3	p1234				
							17.8	3.7	89	6.1	p19				
							9.5	4.7	23	2.4	210				
							15.6	7.7	16	2.5	3170				
20	EGR J0348-5717	57.01	−57.30	−90.40	−46.78	0.63	21.9	7.5	25	4.1	p2	−90.67	−46.85	23.1	3EGJ0348-5708
							4.1	3.2	10	1.5	p4				
							1.4	1.3	17	1.1	p1234				
							1.7	1.3	23	1.3	p19				
21	EGR J0413-1851	63.27	−18.86	−146.07	−43.17	1.26	47.7	15.9	18	4.4	3290	−143.25	−42.75	27.4	3EGJ0412-1853
							12.8	7.4	12	2.2	p3				
							8.4	4.4	17	2.2	p34				
							3.5	2.4	20	1.6	p1234				
							3.5	2.4	20	1.6	p19				
22	EGR J0413-3742	63.40	−37.70	−119.80	−46.58	0.68	9.1	2.6	57	4.2	p1234	−119.77	−46.55	9.1	
							11.3	5.0	26	2.6	p1				
							8.2	3.2	28	3.2	p3				
							15.6	9.6	9	2.0	p4				
							11.3	5.0	26	2.6	p12				
							9.1	3.1	36	3.7	p34				
							8.6	2.6	54	4.0	p19				
							12.3	5.2	28	2.8	290				
							6.2	4.3	9	1.8	3290				
							11.6	4.8	23	3.0	335+				
23	EGR J0423+1723	65.94	17.40	178.27	−21.95	0.50	11.8	2.6	170	5.0	p1234	179.25	−22.12	10.0	3EGJ0423+1707
							9.2	3.4	77	3.0	p1				
							21.8	7.2	48	3.5	p3				
							14.4	5.6	42	2.9	p4				
							8.5	3.2	78	2.8	p12				
							17.1	4.4	88	4.4	p34				
							9.1	2.4	148	4.1	p19				
							21.9	10.6	21	2.5	36+				
							26.3	14.3	14	2.2	3170				
							19.0	12.6	12	1.8	4130				
24	EGR J0425-0032	66.33	−0.54	−165.20	−32.28	0.41	17.6	3.0	156	7.1	p1234	−164.98	−32.38	15.0	3EGJ0422-0102
							23.4	4.3	107	6.7	p1				
							21.0	12.8	10	2.0	p2				
							11.3	4.6	32	2.9	p4				
							23.0	4.1	115	7.0	p12				
							9.4	4.2	37	2.5	p34				
							16.3	2.9	153	6.8	p19				
							49.5	10.6	51	6.6	210				
							13.0	7.4	15	2.1	290				
25	EGR J0430+0339	67.58	3.65	−168.48	−28.95	0.51	8.3	2.3	104	4.0	p19	−168.56	−29.08	12.0	3EGJ0429+0337
							6.7	3.3	38	2.2	p1				
							9.0	6.9	15	1.5	p3				
							6.6	4.5	21	1.6	p4				
							6.7	3.1	42	2.4	p12				
							6.9	3.7	33	2.0	p34				
							6.9	2.4	77	3.2	p1234				
							14.2	9.5	12	1.7	p56				
							30.3	14.5	17	2.6	p789				
							12.1	8.5	10	1.7	210				
							21.4	8.6	24	3.0	419+				
26	EGR J0433+2906	68.34	29.11	170.47	−12.64	0.17	24.8	5.2	126	5.4	p34	170.48	−12.63	27.2	3EGJ0433+2908
							6.7	3.0	82	2.3	p1				
							15.7	11.4	15	1.5	p2				
							22.0	7.7	52	3.2	p3				
							28.4	7.2	77	4.6	p4				
							7.2	2.9	96	2.6	p12				
							12.3	2.6	226	5.2	p1234				
							10.3	2.5	198	4.5	p19				
							12.4	8.9	18	1.5	36+				
							8.8	6.8	21	1.4	2+				
							37.7	16.5	23	2.7	4130				

Table A.1. continued.

Num	Name	*RA*	Dec	l	b	θ_{95}	*F*	σ_F	Cnts	$\sqrt{TS}$	*vp*	$l_{\rm sys}$	$b_{\rm sys}$	$F_{\rm sys}$	3EG
27	EGR J0442-0027	70.71	−0.46	−162.61	−28.51	0.50	78.3	10.1	139	10.8	p3	−162.63	−28.51	79.6	3EGJ0442-0033
							21.6	4.0	118	6.6	p34				
							11.2	2.5	123	5.0	p1234				
							32.0	15.2	14	2.8	p789				
							11.8	2.4	143	5.7	p19				
28	EGR J0450+1145	72.55	11.76	−172.76	−20.29	0.39	101.1	18.9	69	7.2	36+	−172.53	−20.33	94.4	3EGJ0450+1105
							18.4	3.6	153	5.9	p1				
							12.6	8.7	14	1.6	p2				
							9.5	5.8	27	1.8	p3				
							5.6	3.9	25	1.5	p4				
							17.8	3.3	169	6.2	p12				
							6.8	3.3	49	2.2	p34				
							13.1	2.4	218	6.2	p1234				
							6.0	5.1	17	1.2	p56				
							11.8	2.1	248	6.4	p19				
							16.0	5.7	46	3.3	2+				
							12.0	9.2	12	1.4	4130				
29	EGR J0456-2334	74.15	−23.57	−136.15	−35.04	0.69	14.6	4.2	46	4.4	p1	135.75	−34.95	14.3	3EGJ0456-2338
							6.1	5.4	8	1.3	p4				
							14.6	4.2	46	4.4	p12				
							8.5	2.6	56	3.9	p1234				
							8.5	2.5	56	3.9	p19				
							14.7	4.2	46	4.4	290				
30	EGR J0502-0124	75.60	−1.40	−158.96	−24.75	0.36	10.7	2.2	141	5.5	p1234	−158.96	−24.75	11.3	3EGJ0500-0159
							10.9	3.6	60	3.5	p1				
							18.5	5.8	47	3.8	p3				
							7.4	3.4	33	2.4	p4				
							9.9	3.3	61	3.4	p12				
							11.5	3.0	80	4.3	p34				
							10.3	2.2	145	5.5	p19				
							8.8	6.4	15	1.5	2+				
							35.3	10.4	36	4.4	290				
							27.1	11.6	16	3.2	4130				
31	EGR J0509+0550	77.41	5.84	−164.70	−19.52	0.44	8.7	1.9	180	5.1	p19	−164.70	−19.52	6.6	
							7.3	3.0	58	2.6	p1				
							16.4	10.7	17	1.7	p2				
							11.4	5.0	37	2.6	p3				
							8.2	3.5	42	2.6	p4				
							7.8	2.9	70	2.9	p12				
							8.7	2.9	73	3.4	p34				
							8.1	2.0	140	4.4	p1234				
							11.5	5.7	32	2.3	p56				
							11.0	5.4	31	2.3	2+				
							19.9	9.5	20	2.5	4130				
32	EGR J0512-6148	78.14	−61.81	−88.78	−35.29	0.40	6.3	1.7	86	4.5	p1234	−88.83	−35.26	6.6	3EGJ0512-6150
							7.1	2.3	51	3.7	p1				
							4.5	4.1	10	1.2	p3				
							8.8	3.4	29	3.1	p4				
							5.5	2.1	44	3.1	p12				
							7.0	2.6	39	3.1	p34				
							5.6	1.6	84	4.1	p19				
33	EGR J0515+2316	78.96	23.28	−178.92	-8.68	0.49	225.9	22.8	299	12.6	21	−179.82	−8.54	168.9	3EGJ0516+2320
							16.3	3.4	225	5.2	p1				
							14.0	3.2	213	4.7	p12				
							9.2	2.5	209	3.9	p1234				
							6.8	2.2	192	3.2	p19				
							18.7	10.4	22	2.0	4130				
34	EGR J0529-3608	82.43	−36.14	−119.43	−31.32	0.69	14.2	3.3	77	5.3	p1234	−119.08	−31.17	12.9	3EGJ0530-3626
							16.0	5.7	31	3.5	p1				
							14.0	4.5	39	3.8	p3				
							15.9	5.7	31	3.5	p12				
							13.0	4.0	45	3.9	p34				
							14.1	3.3	77	5.3	p19				
							15.7	5.6	31	3.5	290				
							24.4	6.8	41	4.6	335+				
							23.2	8.5	21	3.6	3355				
35	EGR J0530+1331	82.71	13.52	−168.64	−11.04	0.16	78.5	3.1	2361	31.1	p19	−168.64	−11.05	79.5	3EGJ0530+1323
							98.3	5.3	1125	23.3	p1				
							136.2	16.4	192	10.9	p2				
							30.7	7.3	127	4.7	p3				
							89.3	7.2	478	15.6	p4				
							102.4	5.0	1317	25.6	p12				

Table A.1. continued.

Num	Name	*RA*	Dec	l	b	θ_{95}	*F*	σ_F	Cnts	$\sqrt{TS}$	*vp*	l_{sys}	b_{sys}	F_{sys}	3EG
							64.5	5.2	612	14.9	p34				
							86.1	3.6	1924	29.2	p1234				
							65.4	6.9	381	11.2	p56				
							33.6	18.1	20	2.1	36+				
							136.4	9.3	589	19.1	2+				
							84.3	13.2	123	8.2	4130				
							105.0	16.0	131	8.3	419+				
36	EGR J0531-2934	82.90	−29.57	−126.68	−29.29	1.00	32.8	11.4	21	4.1	3355	−127.33	−27.00	23.3	3EGJ0531-2940
							9.6	4.8	19	2.5	p3				
							9.9	4.3	28	2.8	p34				
							6.3	2.7	32	2.7	p1234				
							6.2	2.7	32	2.7	p19				
							18.1	7.1	22	3.4	335+				
							10.6	8.9	8	1.4	419+				
37	EGR J0534+2159	83.67	21.99	−175.40	−5.77	0.06	230.7	4.3	7030	75.8	p19	−175.43	−5.76	230.3	3EGJ0534+2200
							226.6	6.4	3051	49.4	p1				
							192.2	17.8	298	15.0	p2				
							197.1	11.0	789	24.8	p3				
							195.6	10.4	879	25.7	p4				
							224.0	6.0	3365	51.9	p12				
							201.2	7.6	1710	36.5	p34				
							216.9	4.7	5100	63.6	p1234				
							275.3	11.3	1374	34.2	p56				
							255.4	17.5	501	20.8	p789				
							187.9	22.8	171	11.2	36+				
							241.1	10.6	1150	32.4	2+				
							136.2	16.8	199	10.6	4130				
							209.5	28.6	120	10.2	419+				
38	EGR J0537-6946	84.33	−69.78	−79.73	−31.71	0.39	11.9	2.0	175	7.0	p19	−79.82	−31.76	12.1	3EGJ0533-6916
							9.1	2.6	74	4.1	p1				
							18.8	8.0	22	2.9	p2				
							6.7	6.6	8	1.2	p3				
							11.4	4.1	36	3.3	p4				
							10.5	2.5	97	4.9	p12				
							11.1	3.6	47	3.7	p34				
							11.0	2.1	149	6.3	p1234				
							22.4	9.0	26	3.0	p56				
							11.0	8.1	8	1.6	335+				
							17.2	12.8	7	1.6	3355				
39	EGR J0540+0657	85.06	6.95	−161.66	−12.41	1.07	49.4	13.6	48	4.5	p789	−161.66	−12.38	47.7	
							4.5	4.4	19	1.1	p3				
							4.1	1.9	100	2.3	p19				
40	EGR J0540-4358	85.09	−43.98	−109.99	−30.80	0.37	21.9	2.9	191	9.7	p1234	−110.00	−30.75	24.8	3EGJ0540-4402
							14.3	4.0	58	4.2	p1				
							19.0	4.7	60	5.2	p3				
							46.6	8.4	68	8.1	p4				
							14.1	4.0	58	4.2	p12				
							28.6	4.2	132	9.2	p34				
							21.7	2.9	188	9.6	p19				
							8.4	7.1	10	1.3	290				
							26.1	7.4	33	4.9	3290				
							10.6	5.3	20	2.4	335+				
							11.2	7.0	11	2.0	3355				
41	EGR J0614+4204	93.68	42.08	171.34	11.55	0.37	10.3	2.4	129	4.9	p1234	171.20	11.45	10.6	3EGJ0613+4201
							8.5	3.0	71	3.2	p1				
							19.7	12.2	11	2.0	p2				
							18.5	6.5	31	3.5	p4				
							9.5	2.9	85	3.7	p12				
							11.5	4.3	41	3.1	p34				
							10.3	2.4	130	4.9	p19				
							13.7	6.9	25	2.2	2+				
							18.4	12.3	9	1.8	4130				
42	EGR J0615-3308	93.86	−33.15	−119.76	−21.46	0.51	14.8	3.2	82	5.7	p1234	−119.75	−21.55	14.5	3EGJ0616-3310
							12.7	4.1	37	3.9	p1				
							11.4	5.0	26	2.7	p3				
							38.3	17.6	14	2.8	p4				
							12.7	4.1	37	3.9	p12				
							15.8	5.1	41	3.8	p34				
							14.8	3.2	82	5.7	p19				
							20.5	11.2	9	2.5	440				
							8.9	6.4	11	1.7	290				

Table A.1. continued.

Num	Name	*RA*	Dec	l	b	θ_{95}	*F*	σ_F	Cnts	$\sqrt{TS}$	*vp*	l_{sys}	b_{sys}	F_{sys}	3EG
							19.4	10.4	12	2.4	3290				
							15.8	8.7	15	2.2	335+				
							19.7	12.3	10	2.0	3355				
							28.2	14.1	14	2.5	419+				
43	EGR J0617+2238	94.32	22.65	−171.01	3.08	0.10	46.4	3.1	1225	17.5	p19	−171.00	3.05	48.8	3EGJ0617+2238
							41.2	4.5	492	10.5	p1				
							48.9	14.4	61	3.9	p2				
							47.4	7.9	192	7.0	p3				
							57.7	7.9	216	8.9	p4				
							42.4	4.3	559	11.3	p12				
							52.6	5.6	410	11.2	p34				
							46.7	3.4	981	15.9	p1234				
							42.8	9.0	146	5.4	p56				
							45.8	11.3	91	4.7	p789				
							66.6	21.8	36	3.8	36+				
							35.4	7.1	155	5.7	2+				
							47.6	12.1	69	4.7	4130				
44	EGR J0633+0646	98.28	6.77	−155.18	0.96	0.28	21.3	3.3	368	7.1	p1234	−155.18	−0.95	23.0	3EGJ0631+0642
							17.3	4.7	145	4.0	p1				
							18.3	14.1	14	1.4	p2				
							27.7	7.1	109	4.4	p3				
							23.4	6.6	97	4.0	p4				
							17.9	4.5	164	4.3	p12				
							25.3	4.8	205	5.9	p34				
							24.9	12.4	32	2.2	p56				
							20.2	3.1	393	7.1	p19				
							17.1	7.3	53	2.5	2+				
							25.1	12.1	33	2.3	419+				
45	EGR J0633+1750	98.44	17.84	−164.94	4.27	0.04	400.9	5.4	9018	126.5	p19	−164.94	4.27	403.9	3EGJ0633+1751
							373.7	8.3	3371	74.9	p1				
							444.3	26.3	463	28.8	p2				
							386.6	12.4	1582	52.9	p3				
							353.4	12.0	1376	50.2	p4				
							381.0	7.9	3835	80.3	p12				
							371.6	8.7	2969	73.1	p34				
							377.9	5.9	6822	108.7	p1234				
							479.2	16.8	1252	48.2	p56				
							485.4	20.4	891	40.7	p789				
							375.7	12.4	1494	50.7	2+				
							383.3	20.8	543	30.8	4130				
							411.6	32.5	250	22.0	419+				
46	EGR J0722-5121	110.60	−51.36	−97.22	−16.34	0.45	7.9	2.1	107	4.2	p1234	−97.02	−16.25	8.2	3EGJ0725-5140
							9.7	2.9	73	3.9	p1				
							9.1	4.3	33	2.4	p3				
							9.0	2.8	73	3.7	p12				
							5.8	3.2	31	1.9	p34				
							7.8	2.1	105	4.1	p19				
							20.5	7.2	37	3.4	3385				
47	EGR J0723+7134	110.86	71.58	143.72	28.15	0.32	19.4	1.9	358	13.1	p19	143.71	28.17	19.2	3EGJ0721+7120
							20.3	3.4	115	7.5	p1				
							15.7	3.4	76	5.7	p2				
							10.8	4.0	37	3.2	p3				
							27.6	6.8	47	5.4	p4				
							17.8	2.4	187	9.3	p12				
							16.4	3.5	84	5.8	p34				
							17.4	2.0	271	10.9	p1234				
							30.9	5.5	89	7.6	p56				
							10.7	4.0	36	3.2	319+				
48	EGR J0726-4715	111.74	−47.26	-100.78	−13.98	0.50	16.7	3.6	113	5.4	p1	−100.82	−14.73	17.7	3EGJ0724-4713
							15.6	3.4	114	5.2	p12				
							10.1	2.5	124	4.5	p1234				
							9.7	2.5	120	4.4	p19				
49	EGR J0737+1720	114.43	17.34	−157.84	17.84	0.59	13.0	2.8	97	5.6	p1234	−157.83	17.85	13.1	3EGJ0737+1721
							11.6	3.5	54	3.9	p1				
							27.2	22.5	7	1.4	p2				
							15.5	6.4	22	3.0	p3				
							12.0	6.5	13	2.2	p4				
							12.4	3.5	61	4.1	p12				
							13.8	4.6	35	3.7	p34				
							12.6	2.8	96	5.5	p19				
							17.2	9.2	10	2.5	4130				

Table A.1. continued.

Num	Name	*RA*	Dec	l	b	θ_{95}	F	σ_F	Cnts	$\sqrt{TS}$	*vp*	$l_{\rm sys}$	$b_{\rm sys}$	$F_{\rm sys}$	3EG
50	EGR J0743+5438	115.87	54.65	163.16	29.20	0.53	24.3	4.7	82	6.6	227+	163.13	29.21	23.9	3EGJ0743+5447
							21.5	4.3	83	6.3	p2				
							10.9	2.7	86	4.8	p12				
							7.9	2.2	79	4.1	p1234				
							16.9	11.2	10	1.9	p56				
							8.5	2.2	89	4.5	p19				
51	EGR J0807+4856	121.79	48.94	170.20	32.24	0.59	10.8	2.6	82	5.0	p12	170.34	32.30	10.8	3EGJ0808+4844
							10.9	3.5	47	3.7	p1				
							10.7	3.9	35	3.4	p2				
							26.4	24.8	3	1.4	p4				
							10.0	2.4	88	4.9	p1234				
							9.9	2.4	87	4.9	p19				
							12.4	4.1	37	3.8	227+				
52	EGR J0807+5123	121.86	51.39	167.32	32.49	0.70	9.9	2.6	81	4.5	p12	167.12	32.86	10.0	3EGJ0808+5114
							12.9	3.6	58	4.3	p1				
							6.9	3.7	26	2.1	p2				
							8.6	2.3	84	4.3	p1234				
							8.6	2.3	84	4.3	p19				
							3.8	3.7	13	1.1	227+				
53	EGR J0812-0624	123.11	−6.41	−131.70	14.79	0.70	20.6	4.6	73	5.5	p19	−131.77	14.79	18.6	3EGJ0812-0646
							21.5	5.3	60	5.1	p1				
							129.8	86.1	5	2.4	p4				
							21.5	5.3	60	5.1	p12				
							22.3	5.3	63	5.3	p1234				
							14.7	10.3	10	1.7	p56				
							18.1	7.3	25	3.0	440				
54	EGR J0829+0510	127.33	5.18	−140.29	24.10	0.90	17.0	5.1	40	4.1	p1	−139.88	24.87	14.4	3EGJ0828+0508
							17.0	5.1	40	4.1	p12				
							15.6	4.8	40	4.0	p1234				
							15.5	4.8	39	3.9	p19				
							17.1	10.0	13	2.0	440				
55	EGR J0829+2415	127.46	24.25	−160.14	31.67	0.34	26.5	4.0	118	8.7	p1234	−160.29	31.90	25.3	3EGJ0829+2413
							23.0	5.5	52	5.4	p1				
							16.1	6.0	25	3.4	p3				
							81.3	15.8	49	7.8	p4				
							23.1	5.5	52	5.4	p12				
							31.7	6.0	69	7.2	p34				
							26.5	4.0	118	8.7	p19				
56	EGR J0830+7048	127.57	70.81	143.93	33.57	0.57	8.6	1.6	163	6.1	p19	143.52	34.67	7.8	3EGJ0845+7049
							14.7	3.0	96	6.0	p1				
							3.2	2.5	20	1.4	p2				
							9.1	4.4	27	2.3	p3				
							6.6	6.2	7	1.2	p4				
							9.2	2.0	116	5.4	p12				
							8.2	3.6	33	2.6	p34				
							8.9	1.7	148	5.9	p1234				
							6.0	4.5	14	1.5	p56				
							8.8	4.4	26	2.2	319+				
57	EGR J0834-4512	128.70	−45.21	−96.48	−2.88	0.03	747.9	10.9	9417	101.8	p19	−96.49	−2.87	785.9	3EGJ0834-4511
							730.8	14.5	5101	75.5	p1				
							699.8	41.5	616	24.2	p2				
							762.6	19.5	3073	58.6	p3				
							874.4	57.5	467	22.7	p4				
							727.0	13.7	5713	78.9	p12				
							773.2	18.5	3528	62.5	p34				
							744.1	11.0	9244	100.8	p1234				
							91.5	9.1	186	15.7	p789				
							777.6	23.7	2154	49.4	3385				
58	EGR J0852-1224	133.24	−12.40	−120.77	19.98	0.87	41.2	11.1	36	5.1	440	−121.16	19.39	41.7	3EGJ0852-1216
							14.2	4.4	43	4.0	p1				
							14.2	4.4	43	4.0	p12				
							13.5	4.3	41	3.8	p1234				
							13.0	4.3	40	3.7	p19				
59	EGR J0853+2015	133.46	20.25	−153.45	35.65	0.30	12.1	3.1	58	4.7	p1234	−153.67	36.00	10.2	3EGJ0853+1941
							10.9	4.5	27	2.9	p1				
							11.4	5.8	17	2.3	p3				
							18.9	7.5	16	3.5	p4				
							10.8	4.5	27	2.9	p12				
							13.7	4.5	32	3.9	p34				
							12.1	3.1	58	4.7	p19				

Table A.1. continued.

Num	Name	*RA*	Dec	l	b	θ_{95}	F	σ_F	Cnts	$\sqrt{TS}$	*vp*	$l_{\rm sys}$	$b_{\rm sys}$	$F_{\rm sys}$	3EG
60	EGR J0901-3525	135.45	–35.42	–100.87	7.26	0.33	25.5	4.8	146	6.2	p1	–100.69	7.35	23.7	3EGJ0903-3531
							8.4	5.6	26	1.6	p3				
							24.0	4.5	153	6.2	p12				
							8.2	5.6	25	1.6	p34				
							18.7	3.6	178	6.0	p1234				
							18.3	3.5	175	5.9	p19				
61	EGR J0918+4451	139.52	44.85	175.54	44.29	0.47	14.1	2.0	167	8.8	p19	175.53	44.28	14.1	3EGJ0917+4427
							14.1	3.3	64	5.4	p1				
							11.9	3.4	49	4.3	p2				
							19.4	4.7	49	5.5	p3				
							12.8	2.3	111	6.7	p12				
							17.0	4.1	52	5.5	p34				
							14.0	2.0	165	8.7	p1234				
							64.5	62.6	2	1.9	p789				
							14.6	4.0	48	4.7	227+				
62	EGR J0956+6524	149.24	65.41	146.07	43.06	0.73	13.2	3.0	86	5.4	227+	146.02	43.05	12.3	3EGJ0958+6533
							12.1	2.7	95	5.3	p2				
							5.5	1.7	84	3.7	p12				
							4.5	1.5	80	3.2	p1234				
							4.6	1.5	85	3.4	p19				
63	EGR J0957+5513	149.32	55.22	158.85	47.95	0.47	9.7	1.6	161	7.3	p1234	158.85	47.95	8.5	3EGJ0952+5501
							7.0	2.5	43	3.3	p1				
							9.3	2.4	65	4.6	p2				
							20.0	5.0	50	5.1	p3				
							9.5	6.7	9	1.6	p4				
							8.1	1.7	107	5.6	p12				
							16.7	4.0	58	5.2	p34				
							77.0	64.3	3	1.7	p789				
							9.8	1.6	164	7.3	p19				
							8.8	2.7	48	3.8	227+				
							10.6	7.0	9	1.8	4180				
64	EGR J1009+4831	152.39	48.52	167.46	52.19	0.49	5.5	1.4	84	4.5	p19	167.48	52.18	5.6	3EGJ1009+4855
							7.6	2.4	45	3.8	p1				
							4.9	2.4	27	2.3	p2				
							7.2	5.3	7	1.6	p4				
							6.2	1.7	72	4.3	p12				
							2.8	2.5	11	1.2	p34				
							5.2	1.4	79	4.2	p1234				
							47.3	34.7	4	2.2	p789				
							8.6	3.1	34	3.4	227+				
							7.5	5.2	8	1.7	4180				
							5.7	4.1	11	1.6	40				
65	EGR J1021-5831	155.37	–58.53	–75.60	–1.16	0.22	70.5	6.1	1017	12.8	p19	–75.52	–1.13	81.7	3EGJ1027-5817
							57.0	8.9	361	7.0	p1				
							51.5	20.2	59	2.8	p2				
							100.7	13.9	316	8.3	p3				
							62.3	22.4	62	3.1	p4				
							57.0	8.1	427	7.7	p12				
							92.0	11.8	379	8.8	p34				
							68.6	6.7	796	11.3	p1234				
							83.6	15.3	216	6.1	p56				
							118.3	23.5	134	5.8	3385				
66	EGR J1048-5839	162.18	–58.66	–72.46	0.50	0.16	58.0	5.8	766	11.2	p19	–72.31	0.28	56.7	3EGJ1048-5840
							51.0	9.2	251	6.1	p1				
							70.7	19.3	85	4.2	p2				
							65.6	11.6	215	6.4	p3				
							60.5	20.8	58	3.3	p4				
							54.3	8.3	333	7.2	p12				
							63.5	10.1	269	7.1	p34				
							57.6	6.4	596	10.0	p1234				
							62.4	13.8	165	5.0	p56				
67	EGR J1058-5221	164.63	–52.36	–73.98	6.76	0.19	28.7	3.3	387	10.1	p19	–73.91	6.80	29.6	3EGJ1058-5234
							22.5	4.9	127	5.2	p1				
							22.8	9.2	36	2.8	p2				
							30.6	7.1	94	5.0	p3				
							34.9	14.0	26	3.0	p4				
							22.6	4.4	164	5.9	p12				
							32.3	6.4	124	6.0	p34				
							26.1	3.6	288	8.4	p1234				
							33.4	8.2	77	4.8	p56				

Table A.1. continued.

Num	Name	*RA*	Dec	l	b	θ_{95}	F	σ_F	Cnts	$\sqrt{TS}$	*vp*	l_{sys}	b_{sys}	F_{sys}	3EG
68	EGR J1058-6101	164.69	–61.03	–70.29	–1.08	0.34	37.3	5.6	476	7.2	p19	–70.05	–0.99	38.0	3EGJ1102-6103
							46.7	9.7	211	5.3	p1				
							32.6	18.8	36	1.9	p2				
							20.0	10.2	66	2.1	p3				
							32.8	18.5	36	1.9	p4				
							45.3	8.7	254	5.7	p12				
							23.4	8.9	104	2.8	p34				
							35.3	6.2	355	6.1	p1234				
							45.8	13.4	114	3.7	p56				
69	EGR J1104+3813	166.20	38.22	179.75	65.09	0.21	14.1	1.8	194	10.5	p19	179.99	65.16	13.9	3EGJ1104+3809
							19.4	3.3	97	7.9	p1				
							13.2	3.5	46	5.0	p2				
							13.7	3.3	49	5.5	p3				
							16.8	2.4	142	9.2	p12				
							10.7	2.7	52	5.2	p34				
							14.3	1.8	190	10.4	p1234				
							20.6	15.9	5	1.8	p56				
							17.5	3.9	57	6.1	40				
70	EGR J1122-5946	170.55	–59.77	–68.09	1.18	0.31	22.2	4.8	244	5.0	p1234	–68.17	1.20	20.7	
							27.0	7.3	132	4.0	p1				
							9.1	8.1	30	1.2	p3				
							53.1	15.1	74	4.0	p4				
							24.5	6.5	153	4.1	p12				
							20.3	7.3	96	3.0	p34				
							17.7	4.3	238	4.4	p19				
71	EGR J1131-0027	172.75	–0.46	–95.37	56.31	0.41	12.2	3.7	44	4.0	virgo3a	–95.37	56.31	11.6	3EGJ1133+0033
							8.2	3.0	41	3.2	p3				
							6.0	2.5	38	2.8	p34				
							2.9	1.6	38	1.9	p1234				
							2.0	1.5	28	1.4	p19				
72	EGR J1134-1533	173.62	–15.55	–82.98	43.42	0.53	45.1	8.6	66	7.5	virgo2	–82.94	43.49	39.1	3EGJ1134-1530
							3.9	3.2	17	1.3	p1				
							37.7	8.3	55	6.2	p2				
							8.5	6.3	11	1.6	p4				
							12.3	3.2	70	4.6	p12				
							4.0	3.3	13	1.3	p34				
							9.2	2.3	82	4.6	p1234				
							7.9	2.3	70	3.9	p19				
							12.2	9.8	6	1.5	2040				
							7.1	4.9	14	1.6	virgo3a				
73	EGR J1158-1950	179.68	–19.84	–73.67	41.33	0.80	11.4	3.6	40	4.0	p34	–73.66	41.34	10.6	
							9.7	5.2	18	2.2	p3				
							11.5	4.8	19	3.1	p4				
							3.3	1.8	36	2.0	p1234				
							3.0	1.7	34	1.9	p19				
							5.1	5.1	8	1.1	virgo2				
							10.5	5.9	16	2.2	virgo3a				
74	EGR J1201+2915	180.25	29.25	–160.82	78.69	0.10	52.3	11.3	44	7.1	4180	–159.62	78.72	46.4	3EGJ1200+2847
							7.9	5.4	14	1.7	p2				
							8.9	3.0	45	3.5	p3				
							49.3	11.0	41	6.8	p4				
							14.7	3.0	87	6.1	p34				
							6.9	1.8	86	4.4	p1234				
							75.0	21.6	20	5.4	p789				
							8.4	1.8	116	5.5	p19				
							13.6	5.4	26	3.0	virgo3a				
75	EGR J1218-1545	184.71	–15.76	–68.48	46.39	0.42	18.7	5.5	39	4.4	virgo3a	–68.50	47.04	19.4	3EGJ1219-1520
							15.9	4.9	40	4.1	p3				
							2.1	2.0	19	1.1	p12				
							7.4	2.9	40	2.9	p34				
							4.4	1.7	63	2.8	p1234				
							4.3	1.6	74	3.0	p19				
76	EGR J1222+2845	185.74	28.75	–163.19	83.51	0.23	12.5	1.8	179	8.3	p19	–163.19	83.51	8.9	3EGJ1222+2841
							4.6	2.5	22	2.0	p1				
							7.6	4.2	16	2.2	p2				
							14.4	3.4	68	5.2	p3				

Table A.1. continued.

Num	Name	*RA*	Dec	l	b	θ_{95}	*F*	σ_F	Cnts	$\sqrt{TS}$	*vp*	l_{sys}	b_{sys}	F_{sys}	3EG
							26.7	8.9	28	4.0	p4				
							5.9	2.2	41	3.1	p12				
							16.4	3.2	95	6.4	p34				
							11.6	1.9	149	7.6	p1234				
							12.1	7.1	16	1.9	p56				
							33.7	11.8	26	3.7	4180				
							7.7	3.7	21	2.5	40				
							36.7	18.1	9	2.8	2040				
							17.7	5.0	36	4.7	virgo3a				
77	EGR J1225+2115	186.25	21.25	–104.19	81.58	0.07	11.5	1.8	190	7.8	p1234	–104.19	81.58	13.4	3EGJ1224+2118
							9.0	3.0	51	3.5	p1				
							9.2	5.3	22	1.9	p2				
							12.7	2.8	81	5.7	p3				
							10.5	2.6	84	4.7	p12				
							11.7	2.3	99	6.1	p34				
							10.6	1.7	184	7.4	p19				
							11.1	10.3	4	1.4	4180				
							14.4	7.6	20	2.2	virgo2				
							18.0	6.5	30	3.5	40				
							30.4	14.7	16	2.6	2040				
							10.7	3.7	35	3.5	virgo3a				
78	EGR J1229+0203	187.25	2.06	–70.12	64.36	0.26	27.8	1.9	771	17.5	p19	–70.12	64.36	26.5	3EGJ1229+0210
							19.6	3.4	155	6.6	p1				
							15.9	5.1	53	3.5	p2				
							31.0	3.9	202	9.9	p3				
							24.8	4.7	107	6.5	p4				
							18.4	2.9	207	7.5	p12				
							28.1	3.0	305	11.6	p34				
							23.2	2.1	513	13.4	p1234				
							56.2	6.3	241	11.6	p56				
							9.6	7.6	13	1.4	p789				
							15.7	5.2	52	3.5	virgo2				
							33.8	4.9	152	8.9	virgo3a				
79	EGR J1231-1412	187.86	–14.20	–64.38	48.39	0.25	8.3	1.6	170	6.0	p19	–64.38	48.39	9.1	3EGJ1234-1318
							4.0	2.6	23	1.7	p1				
							15.4	4.0	63	4.6	p2				
							6.9	3.4	25	2.3	p4				
							8.4	2.3	83	4.2	p12				
							3.8	2.5	25	1.7	p34				
							6.8	1.7	111	4.5	p1234				
							17.6	4.7	58	4.6	p56				
							22.4	5.7	54	5.1	virgo2				
							26.7	10.1	23	3.3	2040				
80	EGR J1237+0434	189.31	4.58	–66.23	67.20	0.66	9.2	1.4	249	7.3	p19	–66.01	67.15	9.7	3EGJ1236+0457
							10.2	2.7	81	4.5	p1				
							14.3	4.4	46	4.0	p2				
							5.5	2.7	37	2.2	p3				
							9.3	3.5	40	3.2	p4				
							11.4	2.3	126	5.9	p12				
							6.7	2.1	73	3.5	p34				
							9.0	1.6	199	6.7	p1234				
							10.7	4.5	41	2.7	p56				
							14.4	4.4	46	4.0	virgo2				
							15.2	6.8	18	2.8	2040				
							5.3	3.4	24	1.7	virgo3a				
81	EGR J1247-0733	191.75	–7.55	–59.00	55.31	0.24	8.1	1.7	219	5.2	p19	–59.17	55.03	8.9	3EGJ1246-0651
							14.0	4.1	91	3.8	p1				
							4.9	3.3	19	1.7	p2				
							10.9	2.9	114	4.2	p12				
							7.4	1.9	143	4.3	p1234				
							7.0	3.9	43	1.9	p56				
							14.2	8.8	19	1.8	p789				
82	EGR J1256-0552	194.01	–5.87	–54.96	56.98	0.09	83.7	2.5	2388	47.2	p19	–54.96	56.98	86.4	3EGJ1255-0549
							161.7	6.6	1104	37.3	p1				
							6.2	3.5	24	2.0	p2				
							41.9	5.0	176	11.3	p3				
							22.2	3.9	121	7.2	p4				
							104.5	4.5	1114	34.1	p12				
							30.5	3.1	294	12.7	p34				
							70.7	2.8	1434	35.9	p1234				

Table A.1. continued.

Num	Name	*RA*	Dec	l	b	θ_{95}	*F*	σ_F	Cnts	$\sqrt{TS}$	*vp*	l_{sys}	b_{sys}	F_{sys}	3EG
							110.9	5.9	755	26.8	p56				
							132.4	13.5	189	14.6	p789				
							6.0	3.9	18	1.7	virgo2				
							43.6	6.0	128	9.9	virgo3a				
83	EGR J1259-2209	194.92	–22.16	–54.55	40.67	0.58	8.6	2.0	128	4.9	p19	–54.63	40.60	8.0	
							9.6	3.7	43	3.0	p1				
							3.2	3.0	15	1.1	p2				
							20.4	8.2	23	3.1	p3				
							8.9	4.3	27	2.4	p4				
							6.2	2.4	58	2.9	p12				
							12.2	3.9	51	3.7	p34				
							8.0	2.0	108	4.5	p1234				
							13.5	7.5	19	2.1	p56				
							17.9	11.4	9	2.0	2040				
							26.6	10.0	24	3.4	virgo3a				
84	EGR J1309-0535	197.29	–5.59	–48.96	57.00	0.32	6.9	1.6	189	4.9	p19	–48.28	57.28	7.9	3EGJ1310-0517
							12.1	3.8	78	3.5	p1				
							5.1	3.2	19	1.8	p2				
							4.2	3.8	16	1.2	p3				
							6.1	2.9	34	2.3	p4				
							9.9	2.7	100	4.1	p12				
							5.0	2.3	47	2.3	p34				
							7.6	1.8	149	4.7	p1234				
							7.5	3.5	48	2.3	p56				
							6.9	3.8	20	2.1	virgo2				
							9.2	6.2	10	1.8	2040				
85	EGR J1314-3417	198.58	–34.30	–51.70	28.33	0.45	12.6	2.3	156	6.3	p1234	–51.69	28.20	13.1	3EGJ1314-3431
							15.8	4.6	58	4.1	p1				
							15.9	3.9	78	4.8	p2				
							8.9	5.2	17	2.0	p4				
							15.6	3.0	134	6.2	p12				
							6.3	3.5	24	2.0	p34				
							12.6	2.3	156	6.3	p19				
86	EGR J1328-4337	202.07	–43.62	–50.04	18.75	0.37	10.5	2.5	144	4.8	p1234	–50.04	18.75	10.8	3EGJ1324-4314
							5.1	4.2	23	1.3	p1				
							14.4	4.4	64	3.7	p2				
							10.3	5.1	29	2.3	p3				
							7.2	6.2	14	1.2	p4				
							10.5	3.1	94	3.8	p12				
							10.0	4.0	48	2.8	p34				
							10.5	2.5	144	4.8	p19				
							15.9	7.6	22	2.4	314+				
87	EGR J1337-1310	204.45	–13.17	–40.02	48.16	0.63	30.2	6.5	82	5.7	p56	–39.34	47.22	26.5	3EGJ1339-1419
							15.2	8.9	14	2.0	p3				
							9.3	3.5	43	3.0	p4				
							10.5	3.3	58	3.7	p34				
							2.6	1.8	36	1.5	p1234				
							38.2	20.3	12	2.3	p789				
							7.2	1.9	124	4.3	p19				
							5.4	5.0	9	1.2	virgo2				
							23.8	10.3	16	3.1	2040				
							17.6	8.0	19	2.7	virgo3a				
88	EGR J1338+5102	204.54	51.04	105.73	64.50	0.46	8.5	2.5	50	4.0	p1234	105.73	64.50	7.8	3EGJ1337+5029
							4.3	2.7	17	1.8	p1				
							18.4	6.9	23	3.6	p2				
							13.6	8.0	9	2.2	p4				
							7.9	2.7	42	3.5	p12				
							11.4	7.5	8	1.9	p34				
							8.4	2.5	50	4.0	p19				
							6.0	3.8	12	1.9	40				
89	EGR J1345+2912	206.33	29.20	45.98	77.95	0.73	9.9	2.6	61	4.7	p19	46.62	77.52	10.6	3EGJ1347+2932
							11.8	3.8	30	4.0	p1				
							6.2	5.1	9	1.4	p3				
							10.6	3.4	35	3.8	p12				
							5.6	3.9	14	1.6	p34				
							8.3	2.6	47	3.9	p1234				
							39.6	16.5	14	3.4	p56				
							20.9	6.8	24	4.1	40				

Table A.1. continued.

Num	Name	*RA*	Dec	l	b	θ_{95}	F	σ_F	Cnts	$\sqrt{TS}$	*vp*	l_{sys}	b_{sys}	F_{sys}	3EG
90	EGR J1409-0736	212.27	–7.61	–25.88	50.50	0.25	107.2	9.6	234	16.7	p2	–25.89	50.50	100.8	3EGJ1409-0745
							6.8	4.1	27	1.8	p1				
							5.4	3.4	22	1.7	p4				
							43.9	4.5	268	12.9	p12				
							3.8	3.1	18	1.3	p34				
							26.2	2.9	283	11.2	p1234				
							24.6	2.8	292	11.0	p19				
							28.7	15.5	14	2.2	250				
							99.6	12.7	115	11.8	virgo2				
							78.6	18.3	35	6.3	2040				
91	EGR J1414-6224	213.50	–62.41	–47.67	–1.05	0.35	81.8	12.7	358	7.0	p12	–47.46	–0.42	86.5	3EGJ1410-6147
							83.4	14.2	300	6.4	p1				
							75.5	28.8	58	2.9	p2				
							25.5	13.6	85	1.9	p3				
							38.4	17.1	76	2.4	p4				
							29.2	10.6	156	2.9	p34				
							51.7	8.2	502	6.7	p1234				
							49.9	8.1	484	6.5	p19				
							79.8	24.4	88	3.6	230				
							28.2	15.3	74	1.9	314+				
92	EGR J1418-6040	214.72	–60.68	–46.56	0.40	0.22	68.7	11.9	369	6.2	p34	–46.32	0.38	58.1	3EGJ1420-6038
							20.0	13.3	76	1.5	p1				
							64.7	15.1	218	4.5	p3				
							73.5	19.2	147	4.1	p4				
							15.3	12.0	71	1.3	p12				
							43.7	8.5	439	5.4	p1234				
							42.9	8.5	431	5.3	p19				
							53.7	24.3	63	2.3	230				
							59.5	17.2	152	3.7	314+				
93	EGR J1424+3730	216.08	37.50	66.73	67.89	0.85	17.6	5.1	33	4.6	p1	67.37	67.80	17.6	3EGJ1424+3734
							10.2	3.7	30	3.4	p12				
							9.5	3.7	28	3.1	p1234				
							9.4	3.7	27	3.1	p19				
94	EGR J1428-4240	217.16	–42.67	–38.65	16.70	0.62	26.3	5.1	118	6.2	p34	–37.80	17.68	23.1	3EGJ1429-4217
							6.7	4.1	28	1.8	p1				
							25.3	7.0	62	4.4	p3				
							29.0	7.6	60	4.7	p4				
							3.7	3.0	29	1.3	p12				
							11.3	2.7	141	4.8	p1234				
							11.2	2.6	139	4.7	p19				
							38.8	20.1	14	2.4	4235				
95	EGR J1458-1904	224.56	–19.07	–20.00	34.52	0.59	19.9	5.2	58	4.7	p1	–20.30	34.39	19.8	3EGJ1457-1903
							7.9	6.7	9	1.3	p4				
							13.1	3.9	61	3.9	p12				
							9.6	3.1	62	3.5	p1234				
							9.5	3.1	61	3.4	p19				
							33.5	15.4	12	3.0	250				
							14.5	11.8	6	1.5	4235				
96	EGR J1504-1539	226.14	–15.65	–16.04	36.40	0.65	37.5	10.6	32	4.9	3390	–15.97	36.40	38.0	3EGJ1504-1537
							36.4	10.5	31	4.8	p3				
							21.4	6.6	38	4.2	p34				
							6.6	3.1	38	2.3	p1234				
							6.4	3.1	37	2.3	p19				
97	EGR J1512-0857	228.13	–8.95	–8.66	40.30	0.40	18.7	3.7	112	6.0	p1234	–8.64	40.32	20.4	3EGJ1512-0849
							22.9	5.1	83	5.5	p1				
							15.9	7.9	19	2.4	p3				
							14.9	7.2	17	2.5	p4				
							21.9	5.1	81	5.2	p12				
							14.3	5.3	33	3.3	p34				
							18.5	3.7	111	6.0	p19				
							16.7	8.0	20	2.5	3390				
98	EGR J1516-2536	229.18	–25.60	–20.34	26.72	0.69	28.6	8.3	41	4.4	p3	–20.11	27.10	27.5	3EGJ1517-2538
							4.6	3.7	17	1.3	p1				
							6.7	5.0	20	1.5	p2				
							4.8	3.0	32	1.7	p12				
							17.6	5.8	44	3.6	p34				
							8.1	2.7	75	3.4	p1234				
							7.6	2.6	71	3.2	p19				
							25.1	19.8	10	1.5	2260				
							32.9	19.3	12	2.0	3023				
							28.8	13.2	14	2.9	3390				

Table A.1. continued.

Num	Name	*RA*	Dec	l	b	θ_{95}	*F*	σ_F	Cnts	$\sqrt{TS}$	*vp*	$l_{\rm sys}$	$b_{\rm sys}$	$F_{\rm sys}$	3EG
99	EGR J1607+8216	241.84	82.27	116.06	32.03	0.60	9.8	2.5	73	4.6	p12	115.97	32.03	9.5	3EGJ1621+8203
							10.8	3.0	59	4.4	p1				
							8.8	4.9	17	2.0	p2				
							6.1	6.0	7	1.1	p3				
							8.6	2.2	79	4.5	p1234				
							8.4	2.2	77	4.4	p19				
							11.1	4.1	34	3.2	220				
100	EGR J1607+1533	241.99	15.55	29.10	43.10	0.60	39.3	12.2	27	4.3	250	29.55	43.87	39.5	3EGJ1605+1553
							11.1	4.9	29	2.6	p1				
							19.4	9.3	15	2.6	p3				
							8.4	4.5	24	2.1	p12				
							16.6	8.4	14	2.5	p34				
							10.8	4.0	40	3.1	p1234				
							10.5	4.0	39	3.0	p19				
							20.6	9.5	15	2.8	3390				
101	EGR J1608+1051	242.04	10.85	23.37	41.09	0.39	27.5	5.2	93	6.6	p1	23.37	41.09	31.5	3EGJ1608+1055
							27.1	5.2	92	6.6	p12				
							20.4	4.2	90	5.9	p1234				
							20.4	4.2	90	5.9	p19				
							29.1	11.0	22	3.4	250				
102	EGR J1609-1128	242.32	–11.47	0.82	28.44	0.75	83.8	27.4	24	4.2	229+	0.82	28.44	82.1	3EGJ1607-1101
							22.3	9.6	28	2.7	p2				
103	EGR J1615+3426	243.90	34.44	55.52	46.00	0.16	25.6	3.2	189	10.7	p19	55.53	46.01	25.9	3EGJ1614+3424
							4.7	3.7	12	1.4	p1				
							48.1	8.1	83	8.3	p2				
							64.1	28.6	10	3.4	p3				
							79.2	16.5	47	7.1	p4				
							22.3	4.1	93	7.0	p12				
							74.8	14.3	55	7.7	p34				
							30.1	4.1	148	9.9	p1234				
							19.2	5.1	44	4.9	p56				
104	EGR J1617-2610	244.28	–26.17	–9.78	17.28	0.90	136.6	32.9	62	5.1	4230	–9.82	17.16	107.9	3EGJ1612-2618
							21.0	8.1	73	2.8	p2				
							17.4	9.1	45	2.0	p3				
							36.5	12.7	75	3.1	p4				
							8.2	4.6	77	1.8	p12				
							26.3	7.6	122	3.7	p34				
							14.0	4.0	197	3.7	p1234				
							12.3	3.9	183	3.3	p19				
							15.0	11.5	22	1.4	50				
							41.6	15.6	42	3.0	2260				
							43.9	25.3	18	1.9	3390				
105	EGR J1619+2223	244.75	22.39	39.11	42.96	1.23	38.6	13.3	22	4.0	p56	39.05	42.94	32.7	
106	EGR J1625-2505	246.26	–25.09	–7.69	16.69	0.25	21.5	3.4	342	6.9	p19	–7.23	16.30	26.8	3EGJ1626-2519
							21.1	5.1	131	4.5	p1				
							8.0	6.6	29	1.3	p2				
							13.5	8.2	38	1.7	p3				
							44.4	10.5	104	4.9	p4				
							16.1	4.1	159	4.3	p12				
							26.8	6.6	137	4.5	p34				
							19.5	3.5	292	6.1	p1234				
							49.6	15.7	47	3.8	p56				
							41.3	31.3	9	1.6	2230				
							35.6	20.5	16	2.1	229+				
							17.9	13.2	18	1.5	3023				
							25.8	21.6	11	1.3	3390				
							43.2	28.3	15	1.7	4210				
							37.1	16.4	31	2.5	4235				
107	EGR J1625-2958	246.49	–29.97	–11.29	13.26	0.26	255.5	15.0	612	25.0	p4	–11.10	13.15	258.5	3EGJ1625-2955
							12.0	6.1	48	2.1	p2				
							13.4	7.0	36	2.1	p3				
							5.9	3.4	60	1.8	p12				
							120.4	8.2	615	19.7	p34				
							43.0	3.6	662	14.3	p1234				
							74.1	14.0	98	6.7	p56				
							45.7	3.5	763	15.8	p19				
							289.5	35.8	142	11.6	4230				
							81.1	32.3	20	3.2	2230				
							21.4	11.9	24	2.0	2260				
							226.2	34.2	100	9.3	4210				
							242.6	23.1	223	15.7	4235				

Table A.1. continued.

Num	Name	*RA*	Dec	l	b	θ_{95}	F	σ_F	Cnts	$\sqrt{TS}$	*vp*	l_{sys}	b_{sys}	F_{sys}	3EG
108	EGR J1635+3825	248.95	38.43	61.50	42.25	0.24	48.3	3.7	428	18.3	p19	61.50	42.25	46.8	3EGJ1635+3813
							103.3	9.2	235	17.3	p1				
							31.8	6.8	66	6.2	p2				
							43.1	24.1	9	2.4	p3				
							39.5	11.7	33	4.6	p4				
							68.6	5.8	299	17.1	p12				
							39.5	10.5	41	5.1	p34				
							62.8	5.1	339	17.6	p1234				
							26.3	5.1	85	6.6	p56				
							40.9	21.0	10	2.6	p789				
109	EGR J1638-5157	249.61	–51.95	–25.98	–3.34	0.45	61.5	13.9	142	5.0	p2	–25.78	–3.35	46.0	3EGJ1638-5155
							10.8	9.2	43	1.2	p1				
							18.4	14.8	30	1.3	p4				
							28.1	7.7	177	3.9	p12				
							20.2	6.2	195	3.4	p1234				
							62.0	30.2	32	2.3	p56				
							22.3	6.0	226	3.9	p19				
							17.1	15.9	21	1.1	50				
							84.1	61.9	12	1.5	2230				
							53.2	29.8	28	2.0	2260				
							34.9	33.3	14	1.1	4235				
110	EGR J1640-2807	250.17	–28.13	–7.70	12.06	0.43	19.8	5.2	133	4.2	p34	–7.67	12.01	17.9	3EGJ1638-2749
							11.5	5.7	50	2.2	p2				
							20.1	6.6	80	3.4	p3				
							17.2	8.1	47	2.3	p4				
							9.0	2.8	158	3.4	p1234				
							18.7	11.5	26	1.8	p56				
							9.5	2.7	181	3.7	p19				
							10.9	7.5	24	1.6	50				
							24.1	19.5	14	1.4	4230				
							28.2	23.7	8	1.4	2230				
							25.6	19.1	13	1.5	229+				
							23.2	12.3	25	2.1	3023				
							30.3	22.0	14	1.6	4210				
111	EGR J1642+3940	250.51	39.68	63.26	41.12	0.93	34.9	7.8	56	5.8	5190	64.76	39.40	20.0	
							19.6	4.6	63	5.3	p56				
							9.7	5.3	22	2.1	p1				
							6.8	4.7	15	1.7	p2				
							8.5	3.6	38	2.8	p12				
							7.9	3.2	43	2.9	p1234				
							11.8	2.6	106	5.3	p19				
112	EGR J1652-4552	253.10	–45.87	–19.87	–1.13	0.42	92.5	18.2	250	5.5	p3	–19.01	–1.62	68.9	3EGJ1655-4554
							25.1	12.0	134	2.2	p1				
							25.5	15.9	90	1.6	p2				
							25.4	20.7	47	1.3	p4				
							27.6	9.6	245	2.9	p12				
							65.6	13.7	297	5.1	p34				
							39.1	7.9	524	5.2	p1234				
							37.5	30.9	39	1.3	p56				
							38.0	7.6	549	5.2	p19				
							75.2	34.4	59	2.3	230				
							76.2	62.6	17	1.3	229+				
							125.3	44.1	58	3.2	3023				
							66.5	37.2	38	1.9	4235				
113	EGR J1653-0249	253.30	–2.83	15.75	24.58	0.45	13.3	3.5	110	4.3	p1234	15.78	25.19	13.8	3EGJ1652-0223
							31.1	11.2	31	3.4	p2				
							19.7	6.1	63	3.7	p3				
							9.0	4.3	40	2.3	p12				
							19.1	5.6	74	3.9	p34				
							11.6	3.2	105	4.0	p19				
							26.8	10.5	33	3.0	330+				
							24.8	19.8	6	1.6	4230				
							69.0	44.4	6	2.2	2230				
							48.6	20.9	16	3.1	2260				
							17.0	11.4	13	1.8	3390				
114	EGR J1710-4435	257.68	–44.59	–16.88	–2.89	0.11	122.6	6.2	1966	23.4	p19	–16.89	–2.86	121.6	3EGJ1710-4439
							122.6	10.1	699	14.4	p1				
							131.8	13.3	511	11.7	p2				
							106.7	13.8	335	8.9	p3				
							114.4	16.1	242	8.5	p4				
							127.4	8.1	1219	18.6	p12				

Table A.1. continued.

Num	Name	*RA*	Dec	l	b	θ_{95}	*F*	σ_F	Cnts	$\sqrt{TS}$	*up*	l_{sys}	b_{sys}	F_{sys}	3EG
							107.8	10.5	567	12.0	p34				
							122.0	6.4	1810	22.4	p1234				
							134.7	23.0	163	7.0	p56				
							133.1	15.4	334	10.4	50				
							75.4	30.6	40	2.8	4230				
							206.8	53.8	58	4.8	2230				
							149.8	26.9	143	6.7	2260				
							105.7	49.4	30	2.4	229+				
							167.4	36.5	89	5.5	3023				
							117.7	35.5	54	3.9	4210				
							127.8	31.4	72	4.9	4235				
115	EGR J1718-0436	259.74	–4.61	17.68	18.16	0.36	11.4	3.0	157	4.1	p19	17.76	18.13	12.8	3EGJ1719-0430
							11.6	5.0	59	2.5	p1				
							13.7	9.9	18	1.5	p2				
							8.7	5.0	39	1.9	p3				
							16.7	10.8	21	1.7	p4				
							12.8	4.5	82	3.1	p12				
							11.0	4.6	63	2.6	p34				
							11.7	3.2	142	4.0	p1234				
							28.6	20.8	11	1.6	4230				
							17.4	10.3	21	1.9	200				
							19.1	17.2	8	1.3	2260				
							19.5	18.5	8	1.2	229+				
							56.8	20.4	26	3.6	3390				
116	EGR J1721-0827	260.29	–8.46	14.52	15.71	0.48	32.7	9.5	62	4.1	p4	14.56	15.70	33.3	3EGJ1726-0807
							5.6	5.2	28	1.1	p3				
							12.7	4.6	88	3.0	p34				
							6.5	3.0	95	2.3	p1234				
							6.0	2.9	97	2.2	p19				
							11.3	10.3	16	1.2	50				
							41.6	17.7	21	3.0	4230				
							32.5	15.7	28	2.3	3023				
							31.3	21.3	13	1.7	3390				
							38.2	29.6	8	1.5	4210				
117	EGR J1727+0416	261.99	4.28	27.08	20.50	0.77	15.8	3.9	107	4.6	p1234	27.15	20.57	16.2	3EGJ1727+0429
							19.3	5.8	62	3.8	p1				
							14.1	6.0	39	2.7	p3				
							17.8	5.6	62	3.7	p12				
							13.8	5.5	46	2.8	p34				
							13.3	3.4	109	4.3	p19				
							21.0	8.7	30	2.9	330+				
							29.0	8.6	50	4.1	200				
118	EGR J1732-3126	263.06	–31.44	–3.66	1.11	0.25	34.8	5.9	815	6.1	p19	–3.57	1.09	40.4	3EGJ1734-3232
							29.0	10.4	197	2.9	p1				
							23.7	12.5	122	1.9	p2				
							44.2	11.8	277	3.9	p3				
							48.8	15.9	159	3.2	p4				
							27.0	8.0	322	3.5	p12				
							45.5	9.5	433	5.0	p34				
							34.3	6.1	736	5.8	p1234				
							43.9	21.9	86	2.1	p56				
							31.0	13.5	121	2.4	50				
							50.2	22.8	82	2.3	330+				
							25.0	24.1	35	1.1	2260				
							79.6	41.1	40	2.1	4235				
119	EGR J1734-1315	263.55	–13.26	12.02	10.48	0.23	28.1	3.1	593	10.3	p19	12.01	10.52	31.9	3EGJ1733-1313
							14.7	4.7	104	3.4	p1				
							41.1	8.9	126	5.3	p2				
							30.7	5.8	195	6.0	p3				
							43.9	9.3	112	5.6	p4				
							22.6	4.3	229	5.8	p12				
							33.7	4.9	300	7.9	p34				
							27.7	3.2	526	9.6	p1234				
							34.6	10.3	72	3.8	p56				
							19.3	8.7	43	2.4	50				
							23.6	8.0	67	3.3	330+				
							47.3	17.9	32	3.2	4230				
							40.1	14.3	40	3.2	200				
							54.8	31.7	14	2.2	2230				
							30.1	16.2	23	2.1	2260				
							44.6	19.2	30	2.7	229+				

Table A.1. continued.

Num	Name	*RA*	Dec	l	b	θ_{95}	*F*	σ_F	Cnts	$\sqrt{TS}$	*vp*	l_{sys}	b_{sys}	F_{sys}	3EG
							136.0	45.5	31	3.8	2310				
							29.8	14.8	30	2.2	3023				
							77.9	31.2	27	3.0	4210				
							96.1	33.0	26	3.8	4235				
120	EGR J1740+4946	265.09	49.77	76.72	31.57	0.86	21.5	6.2	45	4.3	p1	76.63	31.49	23.7	
							17.1	10.8	12	1.8	p3				
							9.9	3.6	50	3.1	p12				
							14.6	9.8	13	1.7	p34				
							10.5	3.4	62	3.5	p1234				
							8.0	2.8	61	3.1	p19				
121	EGR J1740+5213	265.19	52.22	79.60	31.73	0.37	26.3	5.7	76	6.0	p2	79.53	31.78	26.9	3EGJ1738+5203
							41.0	27.5	6	2.0	p4				
							15.0	3.6	83	5.1	p12				
							14.0	3.3	90	5.1	p1234				
							12.0	2.9	95	4.9	p19				
122	EGR J1743-1002	265.94	–10.04	16.05	10.11	0.63	37.4	10.4	89	4.0	p56	16.34	9.64	29.0	3EGJ1746-1001
							12.1	5.3	82	2.4	p1				
							24.2	10.5	52	2.5	p2				
							14.5	4.7	130	3.3	p12				
							6.7	3.3	117	2.1	p1234				
							10.8	3.1	213	3.6	p19				
							21.0	10.5	38	2.2	50				
							11.3	11.3	16	1.1	200				
123	EGR J1758-3923	269.62	–39.40	–7.71	–7.58	0.98	83.5	18.2	83	5.5	330+	–8.65	–8.43	72.4	3EGJ1800-3955
							19.1	5.9	103	3.5	p3				
							11.1	4.6	88	2.5	p34				
							25.9	13.9	27	2.1	p56				
							3.9	2.7	75	1.5	p19				
							28.4	25.8	10	1.2	2230				
							42.3	22.0	18	2.3	229+				
							40.9	19.8	25	2.4	3023				
124	EGR J1800-2328	270.20	–23.48	6.43	–0.16	0.23	59.2	6.3	1421	9.8	p19	6.40	–0.25	60.0	3EGJ1800-2338
							63.0	11.3	454	5.9	p1				
							34.4	14.7	145	2.4	p2				
							48.6	11.1	382	4.5	p3				
							94.4	17.7	295	5.7	p4				
							53.1	9.0	606	6.2	p12				
							60.5	9.4	664	6.7	p34				
							56.3	6.5	1260	9.1	p1234				
							126.0	27.2	203	5.0	p56				
							55.5	15.1	212	3.9	50				
							67.0	18.6	198	3.8	330+				
							124.2	31.2	125	4.4	4230				
							40.3	28.6	42	1.5	2260				
							39.6	35.2	30	1.2	229+				
							59.9	53.8	20	1.2	2310				
							103.4	32.8	103	3.4	3023				
							97.8	44.5	50	2.4	4210				
							177.7	61.7	51	3.3	4235				
125	EGR J1809-2322	272.42	–23.37	7.52	–1.88	0.16	43.2	5.4	1007	8.4	p19	7.54	–1.78	58.0	3EGJ1809-2328
							38.8	9.7	273	4.2	p1				
							70.5	14.0	275	5.4	p2				
							38.4	9.3	303	4.3	p3				
							32.5	14.2	99	2.4	p4				
							49.5	8.0	541	6.6	p12				
							35.6	7.8	390	4.8	p34				
							42.3	5.6	925	8.0	p1234				
							80.0	24.4	115	3.5	p56				
							35.6	12.8	133	2.9	50				
							50.2	15.2	156	3.5	330+				
							47.6	43.0	18	1.2	2230				
							80.8	27.6	76	3.2	2260				
							96.1	33.1	69	3.2	229+				
							102.9	45.9	41	2.5	2310				
							64.0	52.1	15	1.3	4235				

Table A.1. continued.

Num	Name	*RA*	Dec	l	b	θ_{95}	*F*	σ_F	Cnts	$\sqrt{TS}$	*vp*	l_{sys}	b_{sys}	F_{sys}	3EG
126	EGR J1812-1316	273.04	–13.27	16.66	2.47	0.22	45.6	5.5	923	8.9	p1234	16.76	2.29	46.2	3EGJ1812-1316
							44.7	8.8	350	5.4	p1				
							44.2	14.4	119	3.3	p2				
							40.5	9.2	300	4.6	p3				
							58.3	16.0	133	4.0	p4				
							45.6	7.5	481	6.5	p12				
							46.5	8.0	450	6.2	p34				
							42.9	5.2	970	8.8	p19				
							44.1	15.6	103	3.0	50				
							44.9	12.7	171	3.8	330+				
							86.8	29.0	65	3.4	4230				
							64.2	30.5	40	2.3	2260				
							89.8	33.2	54	3.0	229+				
							59.1	38.2	26	1.7	2310				
							34.7	29.4	25	1.2	3023				
							83.4	52.4	22	1.8	4210				
127	EGR J1814+2932	273.59	29.54	56.52	20.46	0.80	17.3	4.8	63	4.3	p1	56.99	20.79	17.8	
							7.0	3.1	45	2.5	p12				
							5.8	2.7	49	2.3	p1234				
							6.4	2.7	55	2.6	p19				
							22.5	8.6	25	3.2	20				
							15.8	7.5	24	2.5	200				
							10.7	8.0	14	1.5	328+				
128	EGR J1814-6423	273.64	–64.39	–29.98	–20.46	0.41	14.6	3.9	66	4.5	p1234	–29.97	–20.43	15.5	3EGJ1813-6419
							17.4	5.8	40	3.7	p1				
							19.1	8.8	18	2.8	p2				
							13.9	8.7	12	1.9	p3				
							15.7	4.7	51	4.0	p12				
							11.9	7.1	15	2.0	p34				
							14.5	3.9	65	4.4	p19				
129	EGR J1820-7920	275.16	–79.35	–45.39	–25.22	0.44	24.4	5.8	63	5.3	p12	–45.40	–25.24	23.3	3EGJ1825-7926
							22.2	6.6	40	4.3	p1				
							27.0	11.5	21	2.9	p2				
							20.2	10.2	16	2.4	p3				
							18.8	4.4	74	5.2	p1234				
							18.7	4.4	73	5.2	p19				
130	EGR J1822+1654	275.56	16.91	45.03	13.93	0.60	36.3	10.8	42	4.2	328+	44.95	13.90	39.7	3EGJ1822+1641
							32.1	9.9	50	3.8	p3				
							23.6	8.6	43	3.2	p34				
							6.4	3.7	39	1.8	p1234				
							6.6	3.8	41	1.9	p19				
							35.5	23.4	9	1.9	3315				
131	EGR J1825-1325	276.41	–13.43	18.07	–0.50	0.33	83.5	8.8	1840	9.8	p19	18.11	–0.50	145.6	3EGJ1826-1302
							38.0	14.1	307	2.7	p1				
							143.9	28.1	307	5.4	p2				
							101.7	15.4	753	6.8	p3				
							93.1	27.5	201	3.5	p4				
							69.1	12.6	707	5.6	p12				
							99.3	13.5	950	7.6	p34				
							83.2	9.2	1645	9.3	p1234				
							100.7	27.6	228	3.8	p56				
							53.3	25.6	122	2.1	50				
							114.0	21.1	453	5.6	330+				
							150.4	47.5	107	3.3	4230				
							96.1	26.4	211	3.8	200				
							329.5	59.1	178	6.2	229+				
							184.7	55.2	111	3.5	3023				
							273.8	91.7	67	3.3	4210				
132	EGR J1832-2052	278.04	–20.88	12.17	–5.31	0.36	17.7	3.4	392	5.6	p19	12.10	–5.40	20.0	3EGJ1832-2110
							11.5	5.5	90	2.2	p1				
							32.7	10.1	99	3.6	p2				
							18.5	5.7	140	3.4	p3				
							19.3	9.7	48	2.1	p4				
							17.0	4.8	186	3.7	p12				
							18.6	4.9	186	4.0	p34				
							17.7	3.5	370	5.4	p1234				
							25.2	14.7	32	1.8	p56				
							22.2	8.8	75	2.7	330+				
							91.3	24.4	60	4.6	2260				
							39.2	22.7	25	1.9	3023				
							39.1	26.5	15	1.7	4210				

Table A.1. continued.

Num	Name	*RA*	Dec	l	b	θ_{95}	F	σ_F	Cnts	$\sqrt{TS}$	*vp*	$l_{\rm sys}$	$b_{\rm sys}$	$F_{\rm sys}$	3EG
133	EGR J1835+5919	278.86	59.33	88.75	25.08	0.13	69.2	4.3	556	23.1	p19	88.75	25.08	69.4	3EGJ1835+5918
							58.0	7.6	131	10.8	p1				
							68.3	6.1	284	16.1	p2				
							76.7	12.7	76	9.0	p3				
							65.3	4.8	420	19.6	p12				
							77.3	12.7	79	9.1	p34				
							66.5	4.5	495	21.4	p1234				
							100.2	17.9	58	8.5	p789				
134	EGR J1837-0557	279.35	–5.95	26.04	0.40	0.19	72.2	12.5	461	6.1	p34	25.77	0.31	46.8	3EGJ1837-0606
							24.2	10.7	182	2.3	p1				
							64.8	13.8	333	4.9	p3				
							98.9	28.6	123	3.7	p4				
							22.0	10.0	187	2.2	p12				
							43.2	7.8	643	5.7	p1234				
							41.5	20.8	102	2.1	p56				
							43.1	7.3	747	6.1	p19				
							68.5	17.5	228	4.1	330+				
							55.9	50.8	22	1.1	4230				
							29.3	15.6	104	1.9	200				
							140.6	87.5	20	1.8	430				
135	EGR J1838-0420	279.60	–4.34	27.58	0.91	0.71	369.1	71.8	121	5.9	4230	27.44	1.06	310.4	3EGJ1837-0423
							14.9	13.0	110	1.1	p1				
							83.3	34.7	94	2.5	p4				
							14.5	12.3	121	1.2	p12				
							23.4	15.1	140	1.6	p34				
							19.6	9.5	280	2.1	p1234				
							44.3	26.2	110	1.7	p56				
							23.0	9.0	387	2.6	p19				
							40.1	19.0	150	2.2	200				
136	EGR J1847-3220	281.85	–32.34	3.18	–13.34	0.35	19.9	5.2	83	4.4	p2	3.21	–13.30	25.4	3EGJ1847-3219
							8.2	3.0	80	3.0	p12				
							4.5	2.2	81	2.2	p1234				
							4.2	2.1	78	2.0	p19				
							21.1	13.5	14	1.8	2260				
							35.5	18.8	14	2.4	2310				
							15.8	15.1	8	1.2	3023				
137	EGR J1856+0235	284.23	2.59	35.86	–0.04	0.52	165.4	33.5	192	5.4	p56	34.54	–0.71	208.2	3EGJ1856+0114
							51.1	48.5	20	1.1	p2				
							31.2	15.6	118	2.0	p3				
							96.2	42.0	49	2.5	p4				
							42.8	14.7	183	3.0	p34				
							9.0	8.4	105	1.1	p1234				
							22.7	8.3	292	2.8	p19				
							34.3	20.4	78	1.7	330+				
							128.9	87.1	19	1.6	430				
138	EGR J1912-2000	288.06	–20.01	17.08	–13.41	0.44	14.3	2.6	239	6.2	p1234	17.12	–13.37	17.4	3EGJ1911-2000
							14.1	3.9	99	4.0	p1				
							8.8	5.9	23	1.6	p2				
							18.1	4.6	104	4.4	p3				
							11.8	9.4	16	1.4	p4				
							12.7	3.3	122	4.3	p12				
							18.1	4.2	130	4.8	p34				
							13.7	2.6	232	6.0	p19				
							15.9	6.7	45	2.6	330+				
							35.2	19.0	16	2.2	4230				
							11.1	8.3	15	1.5	200				
							27.4	22.3	8	1.4	430				
							30.4	24.3	9	1.4	3023				
139	EGR J1920+4625	290.17	46.42	77.97	14.61	0.73	16.4	4.7	55	4.2	p1	77.98	14.60	16.7	
							5.2	2.3	52	2.5	p12				
							3.3	1.9	45	1.8	p1234				
							3.1	1.9	42	1.7	p19				
							20.3	5.9	48	4.2	20				
140	EGR J1921-2014	290.41	–20.24	17.79	–15.51	0.56	30.5	8.2	55	4.6	50	17.83	–15.51	34.7	3EGJ1921-2015
							3.7	3.3	25	1.2	p1				
141	EGR J1932-3946	293.07	–39.77	–0.91	–24.39	0.45	12.1	3.1	99	4.5	p12	–1.38	–25.12	12.4	3EGJ1935-4022
							16.2	4.5	74	4.2	p1				
							7.6	4.0	27	2.1	p2				
							11.4	8.4	9	1.6	p4				
							4.2	4.1	13	1.1	p34				
							9.2	2.5	103	4.2	p1234				
							9.2	2.5	103	4.2	p19				
							22.2	7.0	46	3.8	50				

Table A.1. continued.

Num	Name	*RA*	Dec	l	b	θ_{95}	F	σ_F	Cnts	$\sqrt{TS}$	*vp*	$l_{\rm sys}$	$b_{\rm sys}$	$F_{\rm sys}$	3EG
142	EGR J1936-1515	294.24	−15.26	24.07	−16.82	0.92	57.9	19.2	26	4.0	430	24.09	−16.76	64.1	3EGJ1937-1529
							7.2	3.4	51	2.3	p1				
							3.8	2.9	34	1.4	p12				
							18.3	9.8	20	2.1	50				
143	EGR J1940-0123	295.08	−1.39	37.32	−11.50	0.73	38.4	10.5	59	4.5	330+	37.32	−11.80	42.9	3EGJ1940-0121
							24.8	7.4	65	3.8	p3				
							24.3	7.0	71	4.0	p34				
							4.3	3.0	44	1.5	p1234				
							3.8	3.0	40	1.3	p19				
144	EGR J1949-3439	297.41	−34.66	5.58	−26.31	0.57	49.5	12.5	46	5.4	420	4.97	−26.29	51.4	3EGJ1949-3456
							16.6	4.5	77	4.4	p1				
							11.6	3.3	86	4.0	p12				
							6.8	2.6	73	2.9	p1234				
							6.8	2.6	73	2.9	p19				
							11.4	8.1	18	1.5	50				
145	EGR J1955-1338	298.78	−13.64	27.53	−20.17	0.76	22.9	6.4	57	4.3	p34	27.46	−19.54	20.2	3EGJ1955-1414
							23.2	7.0	52	4.0	p3				
							16.8	15.6	5	1.3	p4				
							7.2	2.8	68	2.8	p1234				
							7.1	2.8	67	2.8	p19				
							22.3	8.5	33	3.1	330+				
146	EGR J1959+4322	299.78	43.38	78.44	7.18	0.22	18.8	3.9	206	5.3	p12	78.33	7.14	18.5	
							11.4	6.3	44	1.9	p1				
							22.5	5.0	160	5.0	p2				
							7.6	6.1	32	1.3	p3				
							8.1	6.1	34	1.4	p34				
							15.9	3.3	240	5.2	p1234				
							15.7	3.3	238	5.2	p19				
							20.2	19.1	10	1.2	3315				
147	EGR J1959+6322	299.90	63.37	96.32	16.90	0.37	14.6	3.2	114	5.3	p19	96.51	17.00	15.1	3EGJ1959+6342
							14.6	6.8	27	2.5	p1				
							13.4	4.6	51	3.4	p2				
							18.0	9.0	21	2.3	p3				
							13.1	9.4	11	1.6	p4				
							13.6	3.8	77	4.2	p12				
							16.5	6.6	33	2.9	p34				
							14.1	3.3	108	5.1	p1234				
							32.7	28.7	5	1.5	p789				
							20.5	9.9	18	2.5	20				
148	EGR J2010-2424	302.60	−24.41	18.06	−27.53	0.76	16.8	4.4	75	4.5	p1	19.27	−26.18	16.7	3EGJ2006-2321
							7.3	5.2	15	1.5	p3				
							11.4	3.3	77	3.9	p12				
							8.3	5.3	18	1.7	p34				
							10.0	2.8	89	4.0	p1234				
							10.0	2.8	89	4.0	p19				
149	EGR J2019+3722	304.79	37.37	75.43	0.72	0.18	77.6	6.1	1282	14.2	p19	75.45	0.86	81.9	3EGJ2021+3716
							70.2	11.3	322	6.8	p1				
							71.2	9.5	490	8.3	p2				
							85.1	11.4	393	8.4	p3				
							72.0	7.3	826	10.9	p12				
							85.7	11.3	396	8.5	p34				
							75.9	6.1	1221	13.7	p1234				
							147.4	41.4	62	4.2	p56				
							57.5	13.8	180	4.5	20				
							120.9	15.7	329	8.9	328+				
							177.6	34.6	109	6.2	3315				
150	EGR J2020+4019	305.19	40.32	78.04	2.13	0.13	117.0	6.7	1867	20.0	p1234	78.03	2.16	115.0	3EGJ2020+4017
							113.3	12.7	488	10.2	p1				
							117.2	10.1	850	13.2	p2				
							117.5	12.7	516	10.6	p3				
							115.8	7.9	1339	16.7	p12				
							120.4	12.7	529	10.9	p34				
							73.2	53.1	20	1.5	p56				
							116.3	6.6	1888	20.0	p19				
							128.5	15.7	386	9.4	20				
							132.9	17.8	323	8.6	328+				
							72.3	35.2	39	2.2	3315				

Table A.1. continued.

Num	Name	*RA*	Dec	l	b	θ_{95}	*F*	σ_F	Cnts	$\sqrt{TS}$	*vp*	l_{sys}	b_{sys}	F_{sys}	3EG
151	EGR J2025-0810	306.25	−8.17	36.25	−24.49	0.24	25.1	4.0	145	7.9	p1	36.13	−24.37	26.5	3EGJ2025-0744
							22.8	3.8	141	7.5	p12				
							21.7	3.8	134	7.0	p1234				
							21.7	3.8	135	7.0	p19				
							11.1	6.0	17	2.2	200				
							22.9	13.5	14	2.0	430				
152	EGR J2027-4206	306.79	−42.11	−1.20	−35.00	1.12	16.3	4.8	46	4.2	p2	−1.34	−34.97	17.2	
							5.2	3.0	26	1.9	p12				
							5.4	2.8	33	2.1	p1234				
							5.2	2.8	32	2.1	p19				
153	EGR J2032+1226	308.02	12.44	56.25	−15.74	0.68	13.5	3.0	130	5.1	p19	56.29	−16.95	14.9	3EGJ2036+1132
							5.8	3.6	31	1.7	p1				
							50.7	22.1	61	2.6	p2				
							15.4	6.5	34	2.7	p3				
							33.5	14.2	20	3.1	p4				
							10.5	3.6	68	3.3	p12				
							17.5	5.7	49	3.6	p34				
							12.6	3.0	117	4.7	p1234				
							42.8	20.6	15	2.7	p56				
							11.2	6.0	20	2.2	200				
							19.1	7.3	35	3.0	328+				
							47.7	19.3	20	3.1	3315				
154	EGR J2033+4117	308.37	41.30	80.24	0.75	0.22	51.9	6.6	828	8.4	p1234	80.26	0.81	52.1	3EGJ2033+4118
							49.2	12.0	228	4.4	p1				
							49.9	10.1	357	5.3	p2				
							55.6	12.6	232	4.8	p3				
							49.6	7.7	584	6.8	p12				
							56.9	12.5	238	4.9	p34				
							44.4	43.2	18	1.1	p56				
							51.5	6.5	842	8.4	p19				
							48.1	15.7	135	3.3	20				
							79.7	18.2	182	4.8	328+				
							60.3	38.2	31	1.7	3315				
155	EGR J2045+0935	311.45	9.59	55.70	−20.12	0.33	11.5	2.9	98	4.6	p1234	55.60	−20.17	10.1	3EGJ2046+0933
							12.1	3.7	63	3.8	p1				
							16.7	7.2	29	2.7	p3				
							15.1	9.4	12	1.9	p4				
							9.3	3.3	56	3.2	p12				
							17.4	5.8	43	3.6	p34				
							11.3	2.8	100	4.5	p19				
							21.1	11.6	13	2.2	20				
							11.6	7.8	15	1.7	328+				
							14.8	9.1	12	1.9	4100				
156	EGR J2057-4658	314.32	−46.97	−7.06	−40.56	0.28	20.4	5.8	44	4.4	p1	−7.06	−40.56	21.3	3EGJ2055-4716
							10.3	3.4	46	3.5	p12				
							9.1	3.2	45	3.3	p1234				
							51.7	28.1	10	2.7	p789				
							10.4	3.2	53	3.8	p19				
							23.4	7.1	38	4.2	420				
157	EGR J2200-3015	330.00	−30.25	17.73	−52.49	0.38	20.9	2.9	151	9.4	p19	17.72	–52.29	21.1	3EGJ2158-3023
							4.3	3.9	11	1.2	p1				
							17.0	7.2	19	3.0	p2				
							34.0	8.1	39	6.2	p4				
							8.2	3.5	29	2.7	p12				
							31.7	7.9	36	5.9	p34				
							14.4	3.3	68	5.6	p1234				
							22.5	6.3	37	4.8	p56				
							53.5	12.1	46	6.2	p789				
							34.8	8.1	40	6.5	4040				
							6.6	6.4	9	1.1	420				
158	EGR J2202+3340	330.63	33.68	87.10	−17.19	0.45	9.8	2.6	95	4.4	p19	87.00	−17.27	9.8	
							13.0	5.1	35	3.0	p1				
							8.7	5.1	23	1.9	p2				
							14.5	6.2	28	2.7	p3				
							11.5	3.6	62	3.7	p12				
							4.9	3.6	19	1.5	p34				
							9.0	2.6	83	3.9	p1234				
							22.6	12.5	13	2.2	p56				

Table A.1. continued.

Num	Name	*RA*	Dec	l	b	θ_{95}	*F*	σ_F	Cnts	$\sqrt{TS}$	*vp*	l_{sys}	b_{sys}	F_{sys}	3EG
159	EGR J2204+4225	331.01	42.43	92.88	−10.47	0.40	159.6	22.2	97	11.0	p56	92.75	−10.25	160.8	3EGJ2202+4217
							9.1	5.6	27	1.7	p1				
							13.2	5.2	46	2.8	p2				
							23.5	8.4	33	3.4	p4				
							11.5	3.8	75	3.3	p12				
							13.4	5.2	41	2.9	p34				
							12.6	3.1	121	4.6	p1234				
							22.3	3.3	227	8.1	p19				
							34.7	10.2	35	4.4	4100				
160	EGR J2208+2351	332.03	23.85	81.41	−25.57	0.31	12.5	3.6	59	4.2	p12	81.34	−25.58	12.8	3EGJ2209+2401
							14.0	4.2	49	4.1	p1				
							5.7	3.7	15	1.8	p4				
							3.0	2.9	12	1.1	p34				
							7.9	2.3	70	3.9	p1234				
							13.6	8.1	13	2.0	p56				
							8.2	2.2	80	4.2	p19				
							24.8	21.2	4	1.6	260				
							5.8	3.7	15	1.8	4100				
161	EGR J2227+6114	336.76	61.24	106.44	3.08	0.30	30.4	5.3	291	6.3	p19	106.58	3.22	37.7	3EGJ2227+6122
							30.9	10.6	70	3.2	p1				
							29.2	9.0	102	3.5	p2				
							48.0	19.7	37	2.8	p3				
							26.1	12.7	40	2.2	p4				
							30.1	6.9	173	4.8	p12				
							31.3	10.7	72	3.2	p34				
							30.1	5.8	242	5.7	p1234				
							19.5	9.7	30	2.4	p56				
162	EGR J2233-4812	338.46	−48.21	−14.70	−56.03	0.76	10.7	3.3	47	4.0	p19	−15.63	−55.71	10.8	
							23.4	9.0	21	3.5	p2				
							11.8	6.7	12	2.2	p4				
							7.6	3.6	23	2.5	p12				
							11.6	6.7	12	2.1	p34				
							8.6	3.2	35	3.2	p1234				
							29.5	17.4	9	2.3	p789				
							13.4	6.8	14	2.4	4040				
163	EGR J2234+1127	338.61	11.46	77.65	−39.08	0.17	21.7	2.8	204	9.7	p1234	77.66	−39.09	20.5	3EGJ2232+1147
							30.8	4.6	133	8.9	p1				
							19.0	5.6	48	4.1	p3				
							9.7	4.3	25	2.7	p4				
							30.6	4.6	132	8.9	p12				
							13.9	3.5	71	4.8	p34				
							7.5	5.7	14	1.5	p56				
							18.9	2.5	212	9.3	p19				
							49.6	22.7	11	3.0	260				
							23.5	8.9	30	3.2	3200				
							9.7	4.3	25	2.7	4100				
164	EGR J2240-6734	340.13	−67.58	−40.11	−45.00	0.78	12.6	3.9	44	4.0	p12	−40.24	44.55	13.4	3EGJ2241-6736
							15.8	5.4	31	3.7	p1				
							7.9	5.5	12	1.6	p2				
							12.4	3.8	43	3.9	p1234				
							12.2	3.8	43	3.9	p19				
165	EGR J2243+1519	340.96	15.33	82.99	−37.45	0.70	75.8	25.7	21	4.1	260	83.05	−37.42	76.9	3EGJ2243+1509
							9.2	4.8	35	2.1	p1				
							7.7	5.5	19	1.5	p3				
							9.2	4.8	35	2.1	p12				
							4.1	2.7	37	1.6	p1234				
							2.9	2.4	30	1.2	p19				
							13.5	13.1	5	1.3	3360				
166	EGR J2251-1344	342.77	−13.74	52.37	−58.91	0.68	44.4	9.5	46	6.9	4040	52.81	−58.73	45.3	3EGJ2251-1341
							4.9	4.8	6	1.2	p3				
							38.5	8.9	40	6.3	p4				
							20.1	5.0	46	5.4	p34				
							8.6	2.5	51	4.0	p1234				
							8.5	2.5	51	4.0	p19				
							13.2	9.0	7	1.8	3200				
							25.1	21.5	4	1.8	3360				
167	EGR J2253+1606	343.48	16.10	86.06	−38.22	0.19	55.5	4.0	486	18.7	p1234	86.04	−38.21	56.7	3EGJ2254+1601
							76.4	6.8	286	15.6	p1				
							29.7	6.7	74	5.4	p3				
							50.4	6.7	127	10.8	p4				
							76.1	6.8	284	15.6	p12				
							41.3	4.8	207	11.4	p34				
							8.4	6.1	12	1.6	p56				

Table A.1. continued.

Num	Name	*RA*	Dec	l	b	θ_{95}	*F*	σ_F	Cnts	$\sqrt{TS}$	*vp*	l_{sys}	b_{sys}	F_{sys}	3EG
							48.6	3.6	492	18.1	p19				
							86.7	24.0	30	4.9	260				
							25.2	9.6	31	3.1	3200				
							20.9	15.7	8	1.6	3360				
							50.5	6.8	127	10.8	4100				
168	EGR J2256-5022	344.20	−50.38	−21.68	58.13	1.06	22.1	7.1	25	4.4	4040	22.26	−58.11	19.8	3EGJ2255-5012
							17.7	6.0	25	4.1	p4				
							17.5	5.9	25	4.0	p34				
							4.9	2.4	27	2.3	p1234				
							5.2	2.4	30	2.4	p19				
							6.9	6.8	6	1.1	420				
169	EGR J2258-2745	344.54	-27.75	24.91	-64.91	0.37	157.6	26.5	60	9.8	p789	24.91	−64.91	154.8	
							9.5	4.3	21	2.6	p4				
							8.9	4.3	20	2.5	p34				
							4.2	2.5	23	1.9	p1234				
							14.2	2.8	93	6.4	p19				
							8.3	4.4	15	2.2	4040				
							10.5	8.9	6	1.4	420				
170	EGR J2308+3645	347.23	36.76	101.03	21.71	0.96	22.6	7.5	28	4.1	4100	101.04	−21.72	22.7	
							22.3	7.7	28	3.8	p4				
							13.2	5.6	22	2.9	p34				
							5.9	3.0	27	2.2	p1234				
							45.8	44.5	9	1.3	p56				
							5.5	2.9	27	2.1	p19				
							20.5	15.1	7	1.7	260				
171	EGR J2314+4430	348.70	44.51	105.34	−15.04	0.46	38.2	9.3	49	5.5	p4	105.31	−14.94	35.3	3EGJ2314+4426
							28.9	7.8	47	4.7	p34				
							9.0	3.7	46	2.7	p1234				
							9.1	3.7	49	2.8	p19				
							24.8	11.2	17	2.9	4100				
172	EGR J2320-0412	350.02	−4.20	75.37	−58.36	0.58	33.8	10.1	33	4.4	3200	75.54	58.23	34.7	3EGJ2321-0328
							13.7	4.9	31	3.5	p3				
							9.2	3.5	32	3.1	p34				
							3.4	2.2	23	1.7	p1234				
							3.6	2.2	24	1.8	p19				
							17.2	12.7	5	1.7	3360				
173	EGR J2353+3806	358.26	38.11	110.46	−23.34	0.87	37.9	10.2	40	4.9	2110	110.47	−23.34	43.0	3EGJ2352+3752
							36.6	10.0	38	4.8	p2				
							7.7	3.6	28	2.4	p12				
							5.2	3.0	25	1.9	p1234				
							4.9	2.9	23	1.8	p19				
174	EGR J2357+4602	359.38	46.04	113.25	−15.82	0.39	14.1	3.6	68	4.8	p1234	112.93	5.54	12.8	3EGJ2358+4604
							11.7	5.0	28	2.8	p1				
							15.0	6.0	26	3.0	p2				
							21.2	10.0	14	2.8	p4				
							12.8	3.8	53	4.0	p12				
							19.1	9.8	12	2.5	p34				
							13.5	3.5	65	4.7	p19				

Table B.1. The EGR confused sources catalogue

Num	Name	*RA*	Dec	l	b	θ_{95}	F	σ_F	Cnts	$\sqrt{TS}$	*vp*	$l_{\rm sys}$	$b_{\rm sys}$	$F_{\rm sys}$	3EG	EGR
1	EGRc J0225+6240	36.38	62.68	133.49	1.75	0.34	30.2	5.0	344	6.5	p19	133.05	1.64	22.1	3EGJ0229+6151	EGR J0240+6112
							42.3	11.5	100	4.1	p1					
							24.9	10.6	64	2.5	p2					
							23.9	10.2	63	2.5	p3					
							38.1	14.4	55	2.9	p4					
							35.1	7.8	173	4.9	p12					
							29.0	8.3	119	3.8	p34					
							32.4	5.7	292	6.2	p1234					
							21.5	10.6	51	2.2	p56					
							25.4	10.6	65	2.6	2110					
2	EGRc J0818-4613	124.74	−46.23	−97.25	−5.73	0.31	29.8	5.7	368	5.6	p1234	−97.25	−5.73	25.8		EGR J0834-4512
							27.8	7.3	199	4.0	p1					
							44.6	10.8	168	4.5	p3					
							37.5	25.4	24	1.6	p4					
							22.5	6.9	179	3.4	p12					
							44.3	10.0	194	4.8	p34					
							27.9	5.7	348	5.2	p19					
							47.1	13.1	122	3.9	3385					
3	EGRc J0842-4501	130.66	−45.03	−95.78	−1.68	0.26	113.9	10.1	1360	12.2	p19	−95.18	−1.47	67.5		EGR J0834-4512
							98.7	13.7	630	7.7	p1					
							148.7	36.5	135	4.5	p2					
							123.8	17.3	492	7.7	p3					
							192.6	52.9	97	4.0	p4					
							104.9	12.8	765	8.7	p12					
							131.9	16.5	590	8.6	p34					
							114.1	10.1	1343	12.1	p1234					
							120.4	21.0	328	6.2	3385					
4	EGRc J0912+7146	138.15	71.77	141.44	36.44	0.62	7.1	1.6	130	5.1	p19	141.85	36.29	5.5		EGR J0830+7048
							8.2	2.8	53	3.3	p1					
							2.4	2.2	16	1.2	p2					
							12.4	4.5	35	3.3	p3					
							12.7	8.4	9	1.9	p4					
							4.9	1.8	64	3.1	p12					
							12.9	4.0	45	3.9	p34					
							6.7	1.6	111	4.7	p1234					
							8.0	5.2	15	1.8	p56					
							12.2	4.5	34	3.2	319+					
5	EGRc J0927+6054	141.91	60.91	153.55	42.15	0.67	5.1	1.5	81	4.0	p1234	153.38	42.50	4.4		
							4.1	2.4	24	1.9	p1					
							3.9	2.1	30	2.1	p2					
							9.0	4.8	16	2.2	p3					
							16.2	8.3	12	2.6	p4					
							4.0	1.5	54	2.9	p12					
							10.6	4.1	27	3.2	p34					
							5.2	1.5	86	4.0	p19					
							2.7	2.2	17	1.3	227+					
6	EGRc J1038-5724	159.61	57.41	−74.25	0.96	0.40	33.1	5.4	455	6.6	p19	−74.25	0.96	38.6		EGR J1048-5839
							23.9	8.2	129	3.1	p1					
							34.5	17.3	44	2.1	p2					
							35.0	11.3	114	3.3	p3					
							27.1	19.9	25	1.5	p4					
							25.5	7.4	171	3.6	p12					
							33.3	9.8	139	3.6	p34					
							28.3	5.9	307	5.1	p1234					
							43.8	12.9	117	3.7	p56					
							120.5	54.4	24	2.7	p789					
7	EGRc J1233-0318	188.46	−3.30	−65.69	59.28	1.04	10.4	2.9	78	4.1	p1	−64.78	58.36	9.8	3EGJ1230-0247	
							7.3	2.3	79	3.6	p12					
							4.6	1.5	97	3.4	p1234					
							3.2	1.3	90	2.6	p19					
							4.3	3.7	17	1.3	virgo3a					
8	EGRc J1255-0404	193.78	−4.08	−55.30	58.78	0.71	9.3	1.9	272	5.3	p19	−55.24	58.82	8.9		EGR J1256-0552
							11.6	4.7	83	2.6	p1					
							7.9	3.3	43	2.7	p4					
							8.0	3.3	88	2.6	p12					
							3.6	2.4	36	1.6	p34					
							6.4	2.0	134	3.3	p1234					
							15.2	4.6	103	3.6	p56					
9	EGRc J1332-1217	203.04	−12.29	−41.69	49.36	0.56	5.9	1.6	112	4.0	p19	−41.67	49.37	7.5		EGR J1337-1310
							6.9	3.3	33	2.3	p1					
							4.5	2.2	40	2.2	p12					
							3.6	1.7	54	2.3	p1234					
							14.7	4.9	52	3.5	p56					

Table B.1. continued

Num	Name	*RA*	Dec	l	b	θ_{95}	F	σ_F	Cnts	$\sqrt{TS}$	*vp*	$l_{\rm sys}$	$b_{\rm sys}$	$F_{\rm sys}$	3EG	EGR
10	EGRc J1740-2851	265.05	−28.85	−0.55	1.05	0.16	70.6	6.3	1750	11.8	p19	−0.27	1.13	45.7	3EGJ1736-2908	EGR J1747-2852
							52.7	10.8	402	5.1	p1					
							69.5	13.9	350	5.3	p2					
							90.0	12.6	615	7.7	p3					
							70.6	17.0	234	4.4	p4					
							59.7	8.6	757	7.4	p12					
							83.3	10.1	846	8.8	p34					
							69.9	6.5	1595	11.3	p1234					
							84.9	24.0	168	3.8	p56					
							42.1	14.4	169	3.1	50					
							102.8	23.6	210	4.7	330+					
							50.5	29.8	51	1.8	4230					
							62.8	49.4	28	1.4	2230					
							72.4	26.6	97	2.9	2260					
							140.7	31.0	156	5.1	3023					
							66.9	38.1	42	1.9	4210					
							111.5	47.6	51	2.5	4235					
11	EGRc J1747-2852	266.76	−28.88	0.21	−0.24	0.23	86.7	6.0	2158	15.7	p19	−0.01	−0.47	146.2	3EGJ1746-2851	EGR J1740-2851
							78.7	10.4	601	8.2	p1					
							73.8	13.3	360	6.0	p2					
							81.8	11.4	586	7.7	p3					
							132.0	17.1	432	8.7	p4					
							76.6	8.2	958	10.1	p12					
							95.8	9.5	1000	11.0	p34					
							84.8	6.2	1947	14.8	p1234					
							124.3	23.8	240	5.7	p56					
							67.8	13.5	282	5.4	50					
							130.9	21.5	294	6.7	330+					
							91.1	29.5	92	3.4	4230					
							155.0	49.1	70	3.6	2230					
							62.1	25.5	79	2.6	2260					
							56.2	35.1	40	1.7	229+					
							209.4	66.0	49	3.8	2310					
							140.5	39.3	88	4.0	4210					
							149.1	50.7	59	3.3	4235					
12	EGRc J2025+3559	306.48	35.99	75.07	−1.18	0.46	40.8	6.6	459	6.6	p12	75.22	−1.09	40.6	3EGJ2027+3429	EGR J2019+3722
							33.9	10.1	155	3.6	p1					
							43.5	8.7	290	5.4	p2					
							10.5	9.7	47	1.1	p3					
							11.5	9.7	52	1.2	p34					
							32.0	5.5	504	6.2	p1234					
							31.6	5.4	515	6.2	p19					
							31.3	12.6	95	2.6	20					
13	EGRc J2215+0653	333.81	6.89	69.17	−39.16	0.59	18.5	5.7	36	4.1	p4	69.01	−38.58	18.2		
							10.9	3.7	44	3.5	p34					
							3.8	2.1	32	2.0	p1234					
							3.0	1.9	30	1.8	p19					
							18.6	5.7	36	4.1	4100					
14	EGRc J2249+1724	342.39	17.41	85.89	-36.55	0.42	26.2	6.7	63	4.8	p3	85.93	-36.41	24.8	3EGJ2248+1745	EGR J2253+1606
							10.2	5.4	36	2.0	p1					
							9.8	5.4	35	2.0	p12					
							14.5	4.2	73	3.9	p34					
							13.7	3.4	118	4.5	p1234					
							12.9	3.0	128	4.7	p19					
							31.0	9.8	37	4.0	3200					